CHALMERS
UNIVERSITY OF TECHNOLOGY

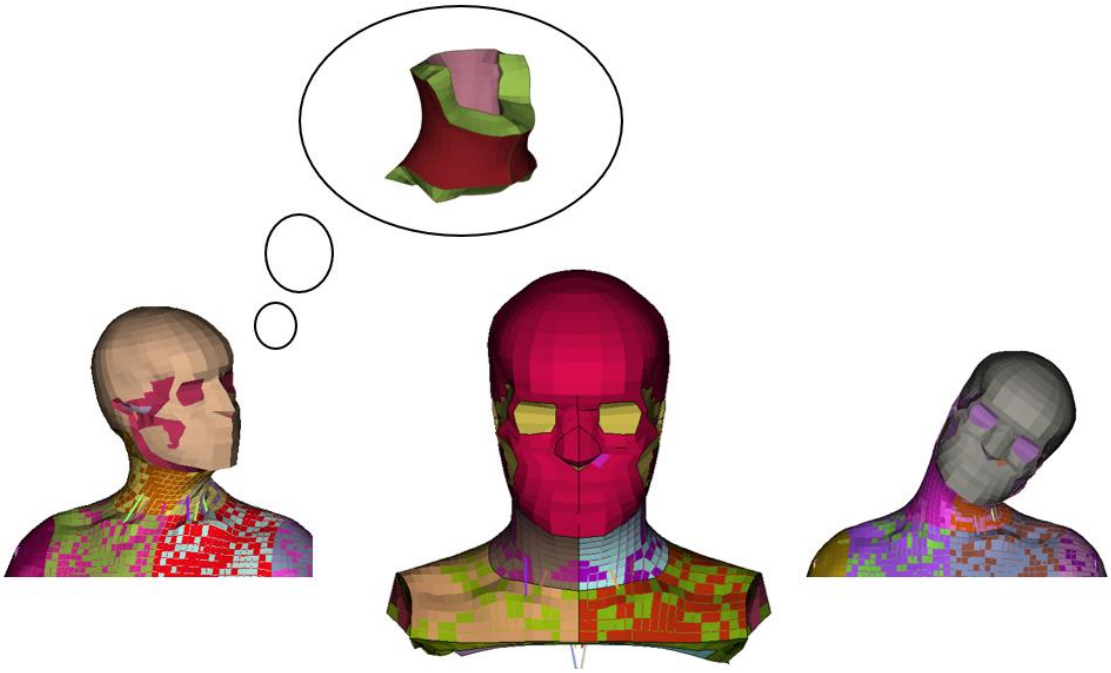

Modification and Validation of the Neck Soft Tissue Models in the SAFER HBM

Master's thesis in Mobility Engineering

MUHAMMED SİRAY HAYRİ

DEPARTMENT OF MECHANICS AND MARITIME SCIENCES

CHALMERS UNIVERSITY OF TECHNOLOGY
Gothenburg, Sweden 2025
www.chalmers.se

MASTER'S THESIS IN MOBILITY ENGINEERING

Modification and validation of the neck soft tissue models in the SAFER HBM

MUHAMMED SİRAY HAYRİ

Department of Mechanics and Maritime Sciences
Division of Vehicle Safety

CHALMERS UNIVERSITY OF TECHNOLOGY
Gothenburg, Sweden 2025

Modification and validation of the neck soft tissue models in the SAFER HBM

MUHAMMED SİRAY HAYRİ

Supervisors: Karl Johan Larsson - Autoliv Research Center,
Ekant Mishra Autoliv Research Center,
Yash Niranjan Poojary - Department of Mechanics and Maritime Sciences / Vehicle Safety Division
Examiner: Johan Davidsson, Department of Mechanics and Maritime Sciences - Vehicle Safety Division

Master's Thesis, 2025
Department of Mechanics and Maritime Sciences
Division of Vehicle Safety

Chalmers University of Technology
SE-412 96 Göteborg
Sweden
Telephone: + 46 (0)31-772 1000

Department of Mechanics and Maritime Sciences
Gothenburg, Sweden June 2025

Modification and validation of the neck soft tissue models in the SAFER HBM
Master's thesis in Mobility Engineering (MPMOB)
MUHAMMED SİRAY HAYRİ
Department of Mechanics and Maritime Sciences
Division of Vehicle Safety
Chalmers University of Technology

Abstract

Cervical spine injuries are common in motor vehicle collisions. Human body models (HBMs) are used in virtual crash simulations to estimate injury risks. The SAFER (Vehicle and Traffic Safety Center at Chalmers) HBM (SHBM) is one such model capable of simulating occupant kinematics and evaluating injury risks. Within the SAFER research initiative, the cervical spine model is being updated under the project "Improving Neck Injury Prediction in Car Crashes Using SAFER HBM." Neck response is influenced not only by the cervical spine but also by surrounding soft tissues such as muscle, fat, and skin.

The aim of this thesis is to investigate and modify the material model and the model geometry of the SHBM neck soft tissue, then validate the biofidelity of the updated neck soft tissue model under both low and high acceleration crash scenarios. Head-neck range of motion (ROM) experiments conducted with human volunteers were replicated using SHBM, and the resulting neck responses were analyzed to understand the effect of the neck soft tissue to neck ROM. A parameter study was carried out to adjust the soft tissue parameters and achieve better agreement between the SHBM neck response and the experimental ROM data. The updated parameters obtained from the parameter study were further calibrated by simulating post-mortem human subject (PMHS) tests using the SHBM under high-acceleration loading conditions. Design modifications such as refining the neck soft tissue mesh and incorporating the nuchal ligament were subsequently implemented to enhance model biofidelity. Finally, a validation study was conducted by simulating both low- and high-speed PMHS crash tests using the original SHBM model geometry with the most promising parameter configurations.

ROM simulations revealed that the SHBM neck exhibited higher resistance to extension and axial rotation compared to experimental results. Following parameter tuning and calibration, a notable reduction in neck moments was achieved. Validation simulations using the updated parameters yielded responses that closely matched experimental reference values.

Although material updates improved neck response, further refinement particularly of the strain-rate-dependent skin model could enhance biofidelity across varying loading rates. Exploring alternative neck flesh material models and refining nuchal ligament design are also promising directions. A key limitation is that SHBM represents only 50th percentile male, limiting generalizability. Extending future investigations to account for population diversity would improve model applicability.

In conclusion, the current SHBM version (v11.1.0) exhibits neck responses under low acceleration conditions that are stiffer than reference values, and softer responses under high acceleration conditions than reference values. The calibrated material parameters resulted in response that was better aligned with experimental data. Minor influence on head forward excursion in validation simulations. The addition of the nuchal ligament improved flexion behavior and is recommended for future versions.

Key words: Neck soft tissue, head-neck response, human body model, SHBM, range of motion, virtual crash test, nuchal ligament.

Contents

Acknowledgements

This thesis work was conducted at Autoliv Research and the Division of Vehicle Safety at Chalmers University of Technology. It was also carried out in collaboration with the team of the SAFER project "Advancing Neck Injury Prediction in Car Crashes Using the SAFER HBM." Additionally, cooperation was established with Dr. Ryan D. Quarrington from the team conducting the "Neck Stiffness and Range of Motion for Young Males and Females" experiments.

Supervision was provided by Dr. Karl Johan Larsson (main supervisor), Ekant Mishra (co-supervisor), and Yash Niranjan Poojary (co-supervisor). Academic and technical support was also provided by Dr. Johan Davidsson (examiner).

All of this work would not have been possible without the support and guidance of several individuals. I would like to express my sincere gratitude to Dr. Johan Davidsson for providing the academic support and guidance I needed throughout this process, and for helping me gain new perspectives in my work through his valuable experience.

I would like to express my endless gratitude and thanks to Karl-Johan Larsson, who gave me the opportunity to work on this thesis, who patiently taught me all the software and tools I would use from the very beginning of the process, who encouraged me and provided me with valuable feedback when I made mistakes, who did not withhold his help and support even outside of working hours when I needed it, who always supported me and encouraged me to do better, who provided me with the best supervision and guidance I have ever received in my life. I could not have done any of this work without him. Super big THANKS!

I am thankful to Ekant Mishra for his helpful supervision and for assisting me promptly whenever I encountered problems. His support played an important role in the success of my work, thanks.

I am also very thankful to Yash Niranjan Poojary for his technical assistance and for patiently helping me solve any technical issues I faced. I greatly appreciate the time he devoted to teaching me and also for his wonderful company, thank you very much.

I would also like to thank Dr. Johan Iraeus, who enabled me to be part of this thesis project and guided me toward taking key steps with his valuable knowledge and insights. I also thank Dr. Jonas Östh for sharing his experience and ideas with me during this time.

I would like to thank Ryan D. Quarrington for his valuable collaboration during this thesis.

Special thanks to the Autoliv Research team for their warm company and the enjoyable lunch conversations during the time I spent working there.

Finally, I would like to express my heartfelt gratitude to my family and friends, who have supported me unconditionally since the very beginning of my master's education.

Gothenburg, June 2025

MUHAMMED SİRAY HAYRİ

Abbreviations

AIS	Abbreviated Injury Scale
ATD(s)	Anthropomorphic Test Devices
C1…C7	Cervical Vertebrae 1…7
CoG	Center of Gravity
FE	Finite Element
GHBMC	Global Human Body Models Consortium
HBM(s)	Human Body Models
ICR	Instantaneous Center of Rotation
IVD(s)	Intervertebral Discs
MPP	Massively Parallel Processing
NASS-CDS	National Automotive Sampling System-Crashworthiness Data System
Occ	The Occipital Condyle
PMHS(s)	Post-Mortem Human Subjects
ROM	Range of Motion
SAFER	Vehicle and Traffic Safety Center at Chalmers
SCF	Seat Cushion Foam
SFA	Scale Factor for Abscissa
SFO	Scale Factor for Ordinate
SHBM	SAFER Human Body Model
T1…T3	Thoracic Vertebrae 1…3
THUMS	Total Human Model for Safety

1 Introduction

Traffic accidents continue to be a global concern, resulting in approximately 1.19 million fatalities and between 20 to 50 million non-fatal injuries annually (World Health Organization 2023). Among the various outcomes of motor vehicle crashes, moderate to severe cervical spine injuries (AIS 2+) have been reported (Forman et al. 2019); however, minor injuries (AIS 1) such as persistent neck pain and disability (symptoms of so called whiplash injuries) occur more frequently (Vos et al. 2008 & Forman et al. 2019). According to five-year (2010–2014) data from the NASS-CDS (National Automotive Sampling System-Crashworthiness Data System) in the United States, whiplash injuries account for 22.71% of vehicle occupants who sustained cervical spine injuries (Freeman and Leith 2020). And whiplash-associated disorders are of high frequency resulting in a correspondingly high societal cost (Cronin et al. 2018).

The evaluation of vehicle safety tools involves both physical and virtual crash testing methods. Physical crash tests utilize anthropomorphic test devices (ATDs, commonly known as crash test dummies), cadavers, and volunteers in low-speed scenarios. Virtual crash tests, on the other hand, frequently employ finite element (FE) models of vehicles, safety devices, and occupants. These virtual occupant models include both models of the ATDs and human body models (HBMs).

While ATDs, and their corresponding models, are utilized in both physical and virtual crash testing, they represent simplified approximations of human anatomy. In contrast, advanced HBMs, such as Total Human Model for Safety (THUMS) (Shigeta et al. 2009), Global Human Body Models Consortium (GHBMC) (Gayzik et al. 2011) and SHBM (Pipkorn et al. 2023), are designed to replicate human anatomy with higher detail than the ATDs to predict the risk of injury in greater detail. Due to their capability to offer realistic and comprehensive representations of the human body during collisions, HBMs are widely employed in vehicle crash safety research and development.

The SHBM, in development since 2008, is a model capable of simulating pre-crash events through active muscle modeling, which represents occupant muscle responses during maneuvers such as braking and lane changes (Larsson 2021). It can also simulate occupant kinematics (i.e., body motion relative to the vehicle) and assess injury risks during high-acceleration crash events.

A current SAFER research initiative, “Advancing Neck Injury Prediction in Car Crashes using the SAFER HBM (“Research Project”),” focuses on updating the SHBM cervical spine model to enhance its capacity for injury prediction. This updated cervical spine model will be integrated into the SHBM. However, the overall neck response in the model is influenced not only by the cervical spine but also by the modeling of soft tissues in the neck, representing the volume of muscles, fat, and skin. These soft tissues potentially play a substantial role in the resulting kinematics of the head and neck, the distribution of loads between the spine and adjacent tissues, and the subsequent injury outcomes, including those affecting the skull and brain. In addition, the modeling of these soft tissues is likely to contribute to improved biofidelity (realistically mimicking the biomechanical behavior of the human body).

1.1 Aim

The aim of this thesis is to investigate, calibrate and validate the neck soft tissue modeling in the SHBM with a focus on achieving biofidelic neck response under both low and high acceleration scenarios. To accomplish this aim, the following objectives were defined:

Objective-1: Modeling Range of Motion (ROM) experiments with SHBM for tuning neck soft tissue modeling

Model ROM (Liu et al. 2024b) test boundary conditions and replicate testing virtually, to compare baseline SHBM predictions to human male volunteers in passive neck range of motion experiments. Additionally, compare cervical spine vertebral rotations to human reference data.

Objective-2: Parameter study to investigate the contributions of the neck soft tissue material modeling on HBM neck ROM results

Modify neck soft tissue material models and material model parameters systematically to understand influence on neck ROM predictions and identify candidate material models and/or parameters that result in improved predictions. Measure influence on vertebral rotations

Objective-3: Evaluation and calibration for high acceleration scenarios

Model high acceleration head and neck experiments previously performed with post-mortem human subject (PMHS) tests (Kang et al. 2018). Evaluate candidate material modelling approaches from the low speed and, if necessary, calibrate parameters for improved predictions also in the high-acceleration scenario.

Objective-4: Updating the model geometry

Modify the neck soft tissue modelling, including geometry (neck circumference, flesh thickness), FE mesh refinement, and material modelling to compare influence of geometry updates in ROM experiment and head and neck sled test

Objective-5: Validation in low-to-high speed crash scenarios

Update SHBM with calibrated material modelling and replicate low speed (9 km/h) (Lopez-Valdez et al. 2017) and high-speed sled tests (40 km/h) (Shaw et al. 2009) previously performed with PMHS. Compare baseline and updated SHBM, focusing on head and neck responses relative to PMHS results.

1.2 Limitations

The study was limited to week 4 through week 24 (2025) and relied on published literature for model adjustments. No new experimental data were collected.

The SHBM represents a 50th percentile male, and the model results were only compared to experimental data for males. While methods such as morphing could be used to adapt the SHBM anthropometry to represent other male and female body sizes, this was considered beyond the scope of this thesis. However, any potential model improvements achieved in this work are likely to benefit SHBMs representing both males and females of varying sizes.

Although the SHBM has the capability to simulate muscle activation by applying forces in the modeled muscles, this study did not account for the influence of muscle activation. As a result, experimental data comparisons were focused solely on passive human responses. Accurate passive neck response is a prerequisite for a valid muscle activation strategy, as the SHBM's muscle controller is calibrated to maintain correct head posture through appropriate muscle activation. If the passive neck response is

inaccurate by e.g., being either too stiff or too soft, the muscle controller would need to compensate by adjusting force activation magnitudes. Other elements that affect neck response, such as the cervical vertebrae and muscle beams, will not be addressed in this study.

2 Background

This section presents an overview of neck anatomy, FE human body modeling, FE modeling of the neck and SHBM.

2.1 Anatomy of the Neck

The neck is the region of the body between the collarbone and the lower jaw (Kohan and Wirth 2014). Its superior (upper) boundary is along the inferior (lower) margins of the mandible and bone features on the posterior (back) aspect of the skull. The posterior neck is higher than the anterior (front) neck to connect cervical viscera (organs) with the posterior openings of the nasal and oral cavities (Drake et al. 2014).

The inferior boundary of the neck extends from the top of the sternum, along the clavicle, and onto the adjacent tip of the shoulder, a bony protection of the scapula. Posteriorly, the inferior limit is a line between the tip of the shoulder and the spinous process of C7 (Drake, Vogl, and Mitchell 2014).

The neck has four major compartments, which are enclosed by an outer musculofascial collar (Drake et al. 2014):

- The vertebral compartment,
- The visceral compartment,
- The two vascular compartments, one on each side.

The vertebral compartment contains the cervical vertebrae and muscles. The visceral compartment contains important glands (thyroid and parathyroid) and parts of the respiratory and digestive tracts that pass between the head and thorax. The two vascular compartments contain the major blood vessels and the vagus nerve (a major nerve involved in regulating heart rate and internal organ function).

The neck also contains two specialized structures related to the digestive and respiratory tracts, the voice box (larynx) and the throat (pharynx) (Drake et al. 2014).

2.1.1 Cervical vertebrae

Cervical spine is the primary structure of the neck, including the vertebrae connected by intervertebral discs (IVDs) and ligaments. The motion of the cervical spine is supported and controlled by 29 muscles (Cronin et al. 2018). The seven cervical vertebrae form the bony framework of the neck. Cervical vertebrae are characterized as small bodies, split (bifid) spinous processes, and transverse processes that contain a foramen (foramen transversarium). They form a longitudinal passage on each side of the cervical vertebral column for blood vessels (vertebral artery and veins). The typical transverse process of a cervical vertebra also has front and back bony bumps (anterior and posterior tubercles) that serve as attachment points for muscles (Drake et al. 2014).

2.1.2 Ligaments

Joints between vertebrae are reinforced and supported by numerous ligaments such as ligamentum flavum and supraspinous ligament which pass between vertebral bodies (Drake et al. 2014). The supraspinous ligament becomes structurally distinct between vertebra C7 and the skull and is called ligamentum nuchae (the nuchal ligament).

2.1.3 Muscles

The majority of the soft tissues surrounding the cervical vertebrae, situated between the skin of the neck and the vertebral column, consist primarily of muscle tissue. These muscles vary in form, ranging from thin sheets to larger, more complex structures (Kohan and Wirth 2014). The neck muscles are an important component in maintaining posture and enable head movements such as flexion, extension, axial rotation, and lateral bending. They also allow for various shoulder blade (scapula) movements (Kohan and Wirth 2014).

2.2 FE Human Body Modeling

Finite element modeling is one of the virtual human body modeling methods. With this method, a mathematical model of the human body is constructed to simulate its mechanical response for vehicle safety applications. This model is then subjected to various boundary conditions such as force, velocity, and displacement in various setups that replicate real-world scenarios such as high- and low-acceleration crashes (or crash tests). Various measurements (kinetic and kinematic, i.e., forces and movements) can be made from certain points (nodes) on the model to understand the biomechanical response of HBMs, to inform engineers about potential human body responses.

There are currently various HBMs available for simulating low and high acceleration virtual crash test setups. Some examples of these are THUMS, GHBMC and SHBM as it is shown in Figure 1. These models represent a 50th percentile male (175cm, 77kg) body model.

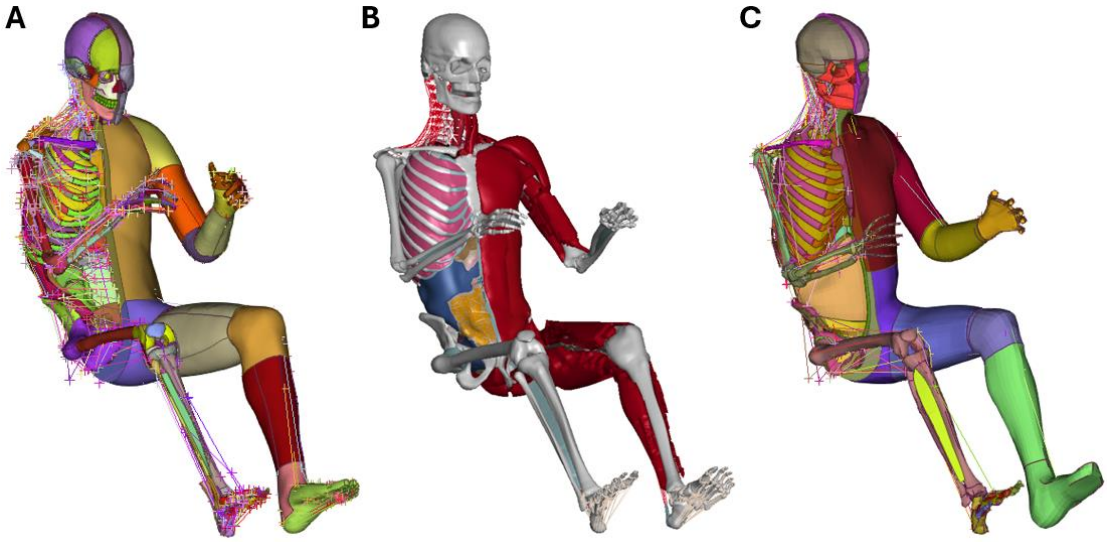

Figure 1: *Some example* HBMs; A: THUMS, B: GHBMC *("GHBMC Licensed Model")*; C: SHBM.

The primary inputs for a FE HBM include geometry (anatomy, anthropometry), material properties (constitutive equations and material data), and boundary conditions, providing kinetic and kinematic responses (Cronin et al. 2018).

2.2.1 Element types of the HBMs

Three types of elements are used in HBMs: beam elements, shell elements, and solid elements. Beam elements are used to represent ligaments and muscles. Shell elements are used to replicate thin structures, such as skin, ligaments, membranes, outer layers of bones, and contact surfaces. On the other hand, solid elements are used to replicate thicker structures such as muscle, fat tissue, bones, and organs.

Since crashes are rapid dynamic events where various parts can come into contact, a FE method with explicit time integration is usually used. Using explicit time integration, the computational time is closely linked to element size, and a trade-off between element size (model level of detail) and the total computational burden always exists. Also, shell and solid elements can have different sizes depending on the structure they are replicated. In this context, the current state of the art for the average length of bone edge elements is 2.5 mm (Iraeus et al. 2020), while this length can increase to 10 mm (Pipkorn et al. 2021) for soft tissue elements such as internal organs, skin, muscles and fat.

Different HBMs are developed with varying focal points, and their designs reflect these specific objectives. For instance, the GHBMC model aims to represent the full-body with high anatomical fidelity (Gayzik et al. 2011). As a result, each muscle group is modeled individually. However, this level of detail leads to smaller element sizes and a significantly higher number of elements, resulting in prolonged computational times (On average 4 times longer than corresponding evaluations using the SHBM, according to Autoliv internal comparisons). To address this, a simplified version of the GHBMC has been developed, in which muscles are grouped and represented by larger regions of coarser solid elements to reduce complexity.

On the other hand, THUMS and SHBM adopt a more simplified approach. SHBM, which builds upon THUMS (Pipkorn et al. 2023), incorporates selective anatomical detailing in critical regions relevant to occupant crash simulations such as detailed skeletal structures and the spine, while employing bulk representations for muscle tissues and abdominal organs. This simplification facilitates a more manageable model structure and aims to achieve reasonable computation times, where a typical target is to complete a 150 ms simulation of a crash event over the night (i.e. 16 hours).

2.3 FE Modeling of the Neck

The structural and functional components of the neck can be divided into hard tissues (bones) and soft tissues. While the cervical vertebrae are classified as hard tissues located in the neck region, the soft tissues comprise muscles, adipose tissue, connective tissues (including ligaments and tendons). For the purpose of human body modeling, the structural components that control the neck kinematics are important to include in a model. Neck models typically consist of the cervical vertebrae connected by IVDs, cervical ligaments, and relevant musculature, which together make up the structural components of the neck (Cronin et al. 2018).

Computational models of the neck may be subject specific, wherein the geometry may be measured from an individual of a specific stature and/or body mass index. Or, models may be created or morphed to achieve a specific stature or subject size (Jolivet et al. 2015). Geometrical data used to generate human body models are measured using a variety of techniques including computerized tomography, magnetic resonance imaging, and external surface measurements (Gayzik et al. 2011). These data are then processed to construct surfaces and finally discretized into a finite element (FE) mesh for each distinguishable anatomic structure (Cronin et al. 2018).

2.3.1 Material models and properties for the neck tissues

The human body comprises biological tissues that typically exhibit nonlinear and viscoelastic response. Although tissues have a common structural makeup

incorporating collagen, elastin (Cronin et al. 2018) and proteins such as actin and myosin (McCuller et al. 2023), the tissues of the neck have different material properties such as elastic stiffness and failure strength; therefore each tissue must be modeled separately with its own numerical formulation (Cronin et al. 2018).

2.3.2 Cervical vertebrae modeling

Various research groups have developed numerous FE models of the neck and cervical spine over the past decades. Notable examples include the SHBM, THUMS, and GHBMC models. In general, solid elements were utilized to represent the vertebral body trabecular bone and IVDs, while shell elements were employed for the cortical bone. The vertebral bodies are connected to each other via ligaments modeled using 1D beam elements and 2D shell elements.

2.3.3 Ligament modeling

Ligaments provide tension-only response between the insertion points of two hard tissues. And various methods have been tried for ligament modeling over the years. There are examples such as 1D tension-only truss elements (Barker et al. 2014), 2D shell elements (Deng et al. 1999) and 3D solid elements (Yang et al. 1998) in different models. Using different types of elements offers certain practical advantages. While 1D elements provide a simpler representation and require less computational effort, 2D and 3D elements allow for more detailed modeling, which generally results in longer computation times.

2.3.4 Muscle modeling

Passive and active musculatures play a strong role in the kinetic and kinematic responses of the neck, particularly in low-severity impact scenarios (Cronin et al. 2018).

In different HBMs, various designs have been designed for muscle structure. However, the muscles of the neck are commonly represented using tension-only, active Hill-type muscle elements (Brolin et al. 2005; Fice et al. 2011). In models such as THUMS and SHBM, active muscle structure is added with 1D beam elements (Östh et al. 2015); passive muscle structure and tissues such as adipose tissue are added to the model with a part consisting of hyperelastic solid elements surrounding the cervical spine.

2.3.5 Skin modeling

In more recent FE models also include a neck skin layer, which can be important for interacting with safety systems such as airbags and seat belts (Cronin et al. 2018). Mostly shell elements are used in neck skin modeling. To imitate viscoelastic human skin, hyperelastic material types are preferred.

2.4 SAFER Human Body Model (SHBM)

The SHBM represents a 50th percentile male occupant and is provided with lumped internal organs and an active muscle package that enables human postural control (Östh et al. 2015).

In the neck part (see Figure 2A and Figure 2B) of SHBM, there are cervical vertebrae and IVDs consisting of solid and shell elements and ligaments consisting of 1D tension-only beam elements connecting them. In addition, 2-nodes active muscle structures consisting of 1D beams surround the neck around the cervical vertebrae as it is shown in Figure 2B. A large part consisting of 3D solid hyperelastic elements, representing the bulk volume of neck muscles and fat, the main focus of this thesis (see Figure 2C),

surrounds the cervical vertebrae together with 1D beam muscle elements, which are attached to the solid hyperelastic elements' nodes. Shell membranes are designed on the inner and outer parts of this solid structure. While the inner shell membrane is used only for contact definitions, the outer membrane has a material model representing the neck skin.

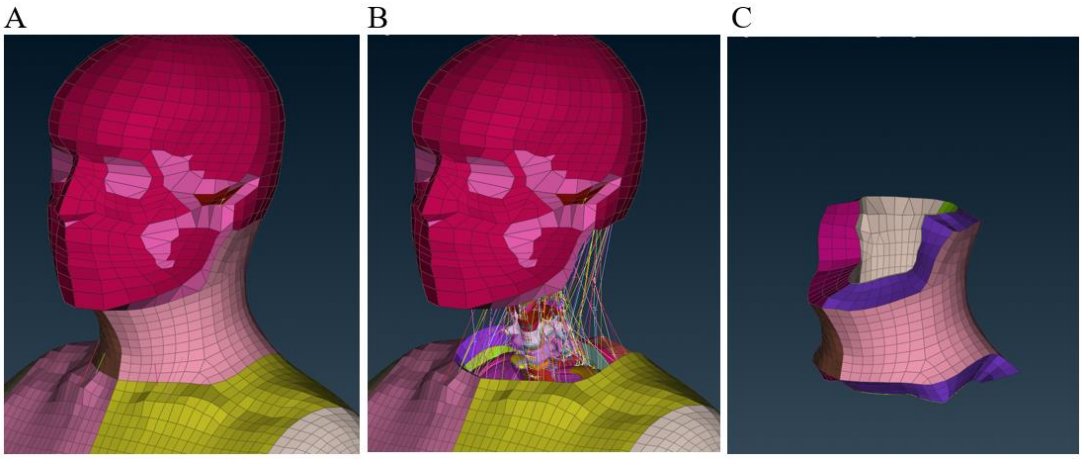

Figure 2: SHBM. A: head + neck. B: neck active muscles beams and cervical vertebrae. C: neck lobe: neck skin + neck flesh (neck passive muscles + adipose).

In the complete neck model of SHBM, it is seen that there are no nerves, glands, veins, respiratory and digestive system pathways. In addition to these, a larger ligament called the nuchal ligament, which connects the vertebrae to the skull, is also missing from the model.

Since neck skin and neck soft tissues are nonlinear materials (Ottenio et al. 2015; Kohan and Wirth 2014), the neck soft tissues of SHBM were modelled with hyperelastic materials as it is shown in Table 1. On the other hand, plastic materials have been used for hard tissues such as cervical vertebrae as it is shown in Table 1.

Table 1: SHBM neck parts material types.

Material Title	Material Type
SHBM Neck Skin	MAT_034: FABRIC
SHBM Neck Flesh	MAT_077_O: OGDEN_RUBBER
SHBM Cervical Vertebrae	MAT_003: PLASTIC KINEMATIC & MAT_034: FABRIC
SHBM Intervertebral Discs	MAT_177: HILL_FOAM & MAT_034: FABRIC

3 Methods

The simulations conducted in this study were performed using *LS-Dyna R12*. *Primer 20.0* and *Ansa v23.1.0* were employed as pre-processors, with *Ansa v23.1.0* specifically utilized for mesh refinement and design modifications. *Meta v23.1.0* served as the post-processor for the analysis of simulation results. Additionally, *Matlab* and *Python* were used for curve generation and to automate certain post-processing tasks.

The computational tools and software listed above were integrated into a structured methodology tailored to address the four main objectives of this study. In the following sections, the methodological approach adopted for each objective is detailed separately, along with a brief presentation of the corresponding findings.

4 Objective-1: Modeling ROM Experiments with SHBM for Tuning Neck Soft Tissue Modeling

Neck stiffness and range of motion experiments conducted by (Liu et al. 2024b) were selected to be recreated in the FE simulations for the slow acceleration scenario. In these experiments, 10 male and 10 female volunteers aged between 20 and 29 were tested. The volunteers participated in head and neck extension, flexion, lateral bending and axial rotation experiments in seated and lying positions. During the experiments, the volunteers were instructed to be relaxed, and muscle activation was monitored to be low, such that the recorded forces and moments represent passive neck responses. The SHBM predictions was compared to the male results.

4.1 Methodology

The objective of this section was to replicate the boundary conditions that produced head and neck movements in the ROM experiments and apply them to SHBM in simulations. To reduce computational cost and minimize the number of elements, the lower portion of the seated SHBM (from the mid-thoracic region to the feet) was excluded. As a result, a truncated model comprising only the head, neck, shoulders, cervical vertebrae, and associated connective tissues was obtained (see Figure 3). The inferior boundary of the truncated parts of the truncated SHBM was fixed.

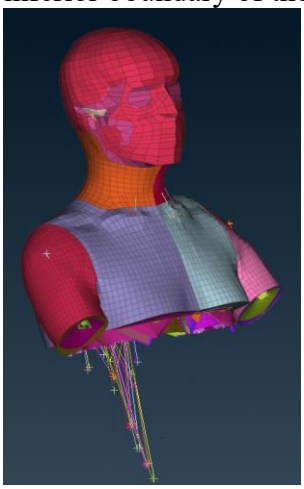

Figure 3: Sectioned SHBM.

Subsequently, four identical instances of this sectioned SHBM were assembled within a single simulation environment without any contact interactions between them (see Figure 4). Each of the SHBMs instances was assigned to replicate one of the ROM experiments (extension, flexion, left lateral bending, left axial rotation), allowing all simulations to be conducted simultaneously within a single solver run (see Figure 5). This setup enabled efficient extraction of neck moment as a function of angular rotation results corresponding to each experimental movement while maintaining a consistent modeling framework. Any modifications applied to the SHBM could be automatically propagated across all four instances, allowing simultaneous evaluation of its effects on each movement scenario.

In the ROM experiment, volunteers neutral neck posture was measured for head-neck positioning. Since this was different for each volunteer, it was not possible to obtain a specific head-neck positioning. Accordingly, it was decided to use the neutral head-neck positioning of the seated SHBM.

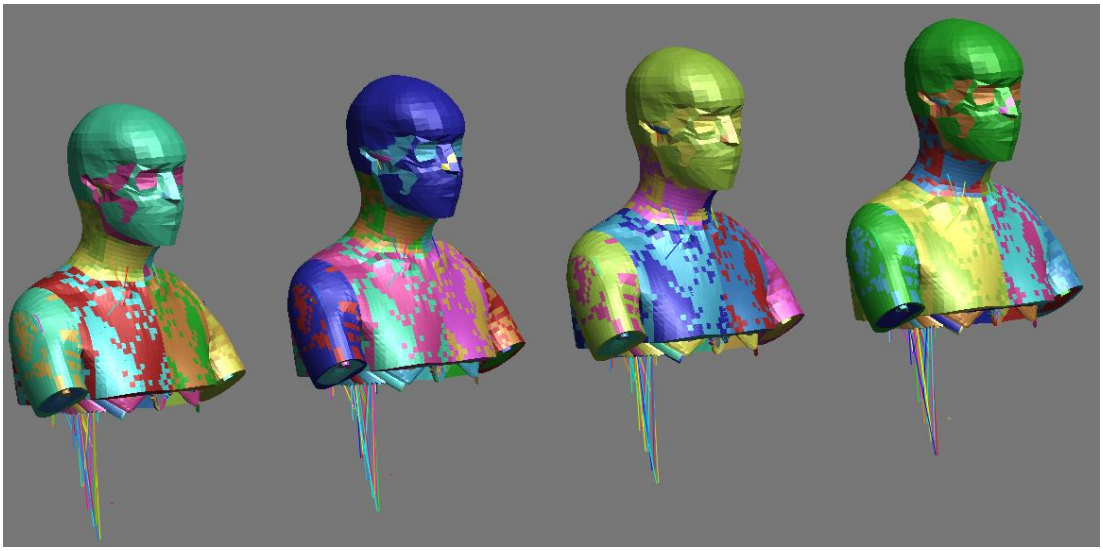

Figure 4: Four SHBMs in one single solver run.

4.1.1 Boundary conditions

Firstly, the SHBMs are constrained at all nodes located at their lowest boundary, beneath the body.

In the ROM experiments, a rectangular support plate was used to stabilize the head during flexion, extension, and lateral bending motions as it is shown in Figure 5. A tangential movement, aligned with the intended head motion, was then applied to this plate. While modeling the plate was not strictly necessary for replicating these movements in the SHBM, three separate plate models were created, each corresponding to flexion, extension, and lateral bending, to enhance visual clarity during post-processing.

To replicate the experimental motions, a prescribed velocity was applied to a node in each plate model, situated at the corresponding location to where force was applied to the plate in the physical experiments. Each plate was constrained to follow a planar motion, to model the sliding on a table that occurred in the experiments. Nodes in the head region of the SHBM were then constrained to their respective plates, ensuring that the head and neck motion followed the applied planar motion.

For axial rotation, the ROM volunteer experiments employed four padded rods to constrain the subject's head while an angular displacement was applied. To replicate this condition, an auxiliary node was created on the head of the fourth SHBM. A rotational velocity curve was assigned to this node to induce angular motion. As with the other configurations, selected head nodes were kinematically linked to the control node to transmit the defined rotational movement.

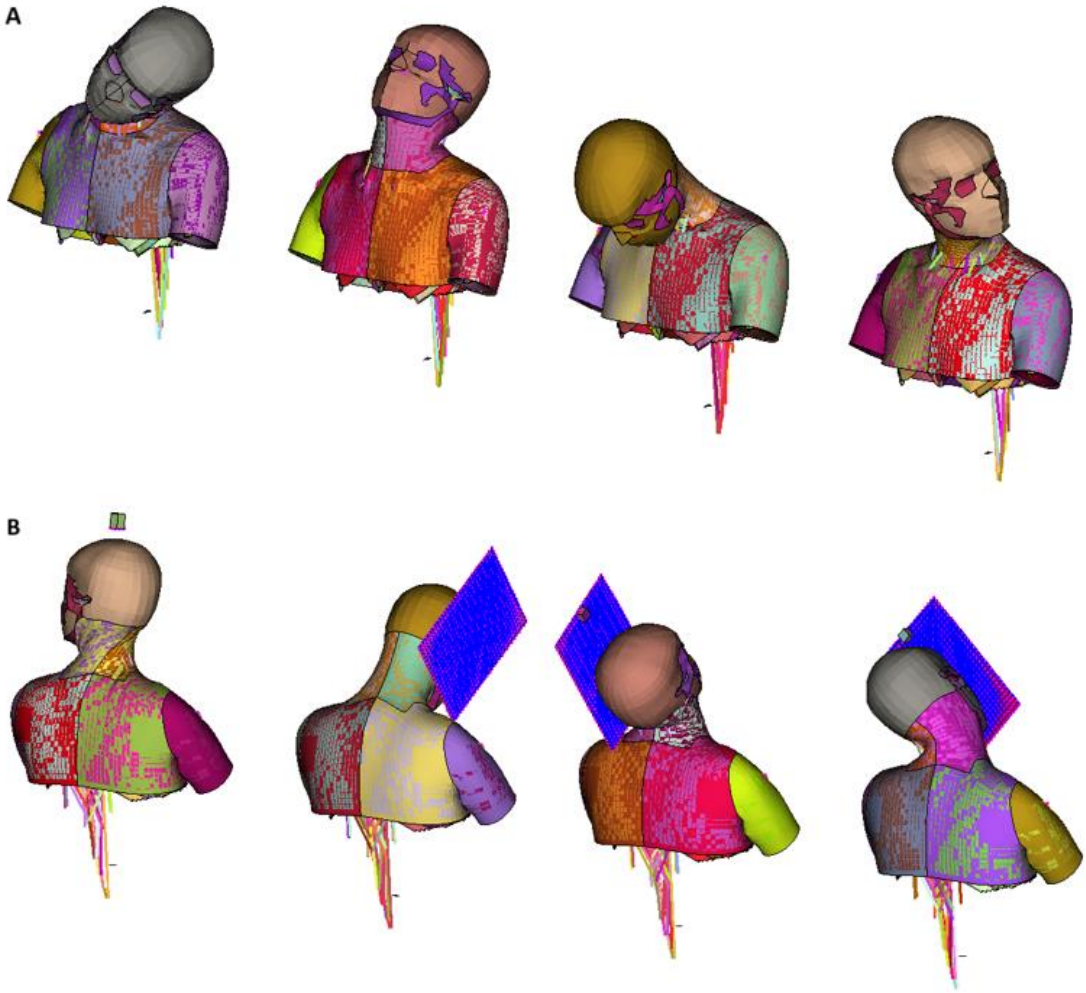

Figure 5: Four SHBMs for each ROM in one single solver. A: Front view (plates hidden) represents lateral bending, extension, flexion and axial rotation respectively. B: Rear view.

4.1.2 Simulation parameters set-up

The ROM experiments were performed at low speeds. In the passive-lying tests, the participant's head was rotated at a rate targeting 10°/s. Considering that some participants rotated their heads up to approximately 100° during axial rotation, a single axial rotation experiment can last around 10 seconds. However, replicating such a long duration (i.e., 10,000 ms) for a parameter study in explicit FE simulations is not feasible, as it would result in a computational time exceeding one week for a single simulation. Therefore, it was necessary to define a more practical simulation time. In order to observe the effect of total simulation time on the results, simulations were conducted using four different termination times: 300 ms, 600 ms, 1000 ms, and 2000 ms. Accordingly, both the translational and angular velocity magnitudes were proportionally scaled as it is shown in Figure 6, to arrive at the same final head and neck rotations regardless of termination time.

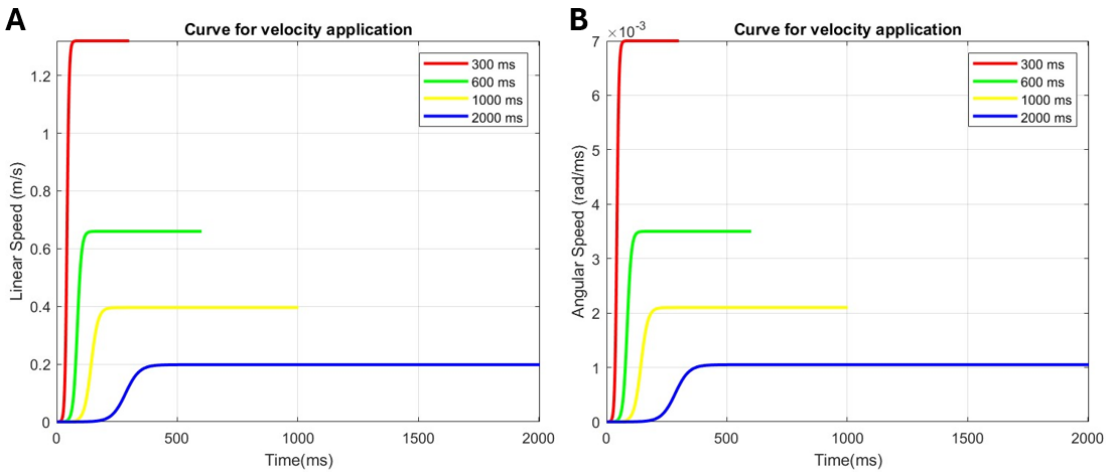

Figure 6: Termination time investigation. A: Bending motions. B: Axial rotation.

Simulations were executed using 32 MPP processors. For post-processing, the time interval for "DATABASE_BINARY_D3PLOT" output files were set to 4 ms.

4.1.3 SHBM neck soft tissue contribution to ROM

In this section, a series of simulations were performed to examine the effect of the neck soft tissue model of SHBM on the ROM results. In the first set, the neck skin was removed from SHBM (see Figure 7B), each representing a different ROM scenario. Subsequently, in a second set of simulations, the neck lobe, representing the underlying muscle and adipose tissue, was also removed from the same four SHBMs (see Figure 7C). These simulations were designed to assess the individual and combined contributions of the neck skin and the overall neck soft tissue to the ROM. It is important to note that in both simulation sets, the muscle beams representing active musculature, without any activation, were retained in the models. The termination time of both simulations was selected as 600 ms. Finally, the results obtained from these simulations were then compared with the results of a simulation run with the nominal version of SHBM (see Figure 7A).

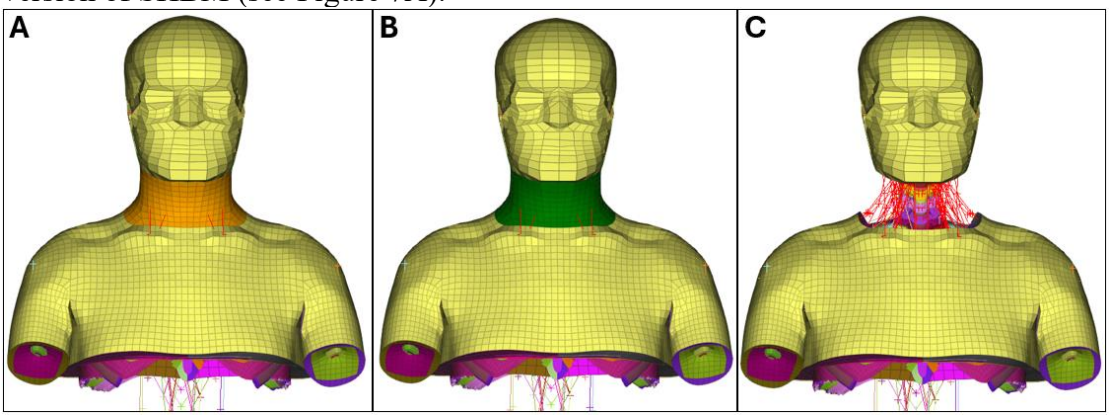

Figure 7: SHBM. A: Nominal. B: No Neck Skin. C: No Neck Lobe (No Neck Skin + No Neck Flesh).

4.1.4 SHBM neck moment vs angle calculation

To calculate the neck moment as a function of angular rotation of the SHBM for the bending motions (extension, flexion and lateral bending), first, the boundary condition force resulting from the applied velocity (i.e., the force needed to obtain the prescribed velocity, which is reported from the solver) was obtained. The moment arm length was then calculated and multiplied by this force.

In ROM experiments, the center of rotation for the bending motions varied continuously. Therefore, the instantaneous center of rotation (ICR) was calculated (Liu et al. 2024a) using the perpendicular bisector theorem (Anderst et al. 2013), and the moment arm length was derived from this center.

The same approach was applied in ROM simulations conducted with the SHBM. For each bending motion and at each time step, the ICR was computed using a custom Python script. The distance between this center and the point of application of the boundary condition force was defined as the moment arm length at each successive time instance. In the experiments, the rotation angle was measured at the rotation point of the center of gravity of the head, and in the SHBM, the rotation angle was measured in the same way.

Finally, the neck moment for each ROM was calculated by multiplying the boundary condition force by the corresponding moment arm length. The resulting moment–angle curves were then compared with the neck moment vs angle data obtained from the ROM experiments.

4.1.5 Neck soft tissue on the angular contribution of segments to ROM

To further validate the biofidelity of the SHBM's neck soft tissue, the angular contribution of individual cervical spine segments, from the first thoracic vertebra (T1) to the occipital condyle (Occ), to the overall ROM was examined. For this purpose, the angular contributions of the Occ–T1 segments were measured in SHBMs under two simulation conditions: (1) the nominal SHBM configuration, and (2) the SHBM without neck soft tissue (i.e., without neck skin and neck flesh; with deactivated muscle beams), as described in the previous section.

In each simulation, the relative rotational displacement between consecutive vertebrae was calculated as a proportion of the total rotational displacement between Occ and T1. These results were then compared with the findings of (Lindenmann et al. 2022), who systematically reviewed the segmental kinematics of the cervical spine.

(Lindenmann et al. 2022)'s review compiled data from studies conducted between 1980 and 2021, focusing on the segmental contributions to cervical spine motion. The review reports the ratio of angular displacement for each segment relative to the total motion between Occ and T1. Importantly, the referenced results are averaged across populations and stratified by age, gender, and other demographic factors. As such, there are no values that correspond specifically to a 50th percentile male, which constitutes a limitation for direct SHBM comparison.

4.2 Results

The results of simulations with different termination times (see Figure 6) were compared, as shown in Figure 8. The total computational times for these simulations were 8 hours, 16 hours, 27 hours, and 61 hours for 300 ms, 600 ms, 1000 ms, and 2000 ms termination times, respectively. For the simulations to be conducted in Objective 2, having a feasible run time was essential. Therefore, the simulations with 1000 ms and 2000 ms durations were considered less practical in this regard.

Another observation from the results was that shorter termination times tend to cause an inertia effect at the beginning of the motion. In particular, the 300 ms simulation appeared too fast for low-speed ROMs. Although the 600 ms simulation also exhibited some initial inertia, it quickly aligned with the curve observed in the longer simulations (1000 ms and 2000 ms).

Consequently, ignoring the initial inertia, a termination time of 600 ms was considered computationally reasonable.

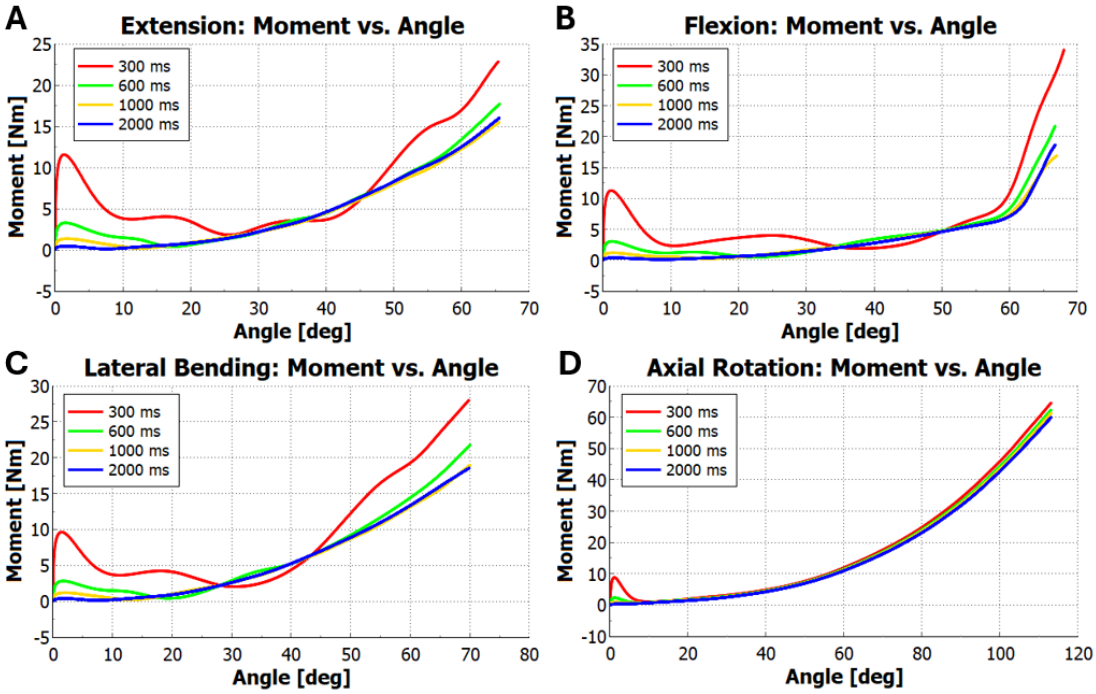

Figure 8: Termination time investigation for ROM. A: Extension. B: Flexion. C: Left lateral bending. D: Left axial rotation.

The obtained results are compared in Figure 9 for the nominal SHBM, the SHBM without neck skin, and the SHBM without neck soft tissue. According to the results, the neck moment of the SHBM decreased when the neck skin was removed as it is shown in Figure 9. Similarly, in some cases, the neck moment decreased by more than half compared to the nominal SHBM when all soft tissue of the neck was removed. Finally, all results were compared with ROM experiment results. These results indicate that the neck skin and neck flesh have a significant effect on the ROM of the SHBM.

The results reported in the review by (Lindenmann et al. 2022) are compared with the angular contributions of each cervical segment in both the nominal SHBM and the SHBM model without neck soft tissue, as illustrated in Figure 10. To define a reference range, the maximum values for each segmental contribution from (Lindenmann et al. 2022)'s data were combined to construct the "(Lindenmann et al. 2022) Max" curve, while the minimum values were similarly compiled to create the "(Lindenmann et al. 2022) Min" curve. Together, these curves form a corridor that represents the measurement bounds.

Analysis of the results reveals that the neck soft tissue in the SHBM significantly affects the angular contributions of the cervical segments to overall head rotation, particularly in flexion and extension. It induces unintended segmental rotations between the Occ–C1 and C1–C2 joints. This behavior is attributed to the high stiffness of the SHBM neck

flesh. The solid neck flesh elements apply compressive forces to the Occ, C1, and C2 vertebrae, which hinders smooth rotational motion.

On the other hand, the influence of neck soft tissue on lateral bending and axial rotation appears to be more limited. In these motions, the nominal SHBM results closely align with those from the corridor. The only notable deviation is observed in the C1–C2 segment during axial rotation, where the relative angular displacement is lower than expected. However, since this discrepancy is also present in the model without neck soft tissue, it cannot be attributed to soft tissue effects.

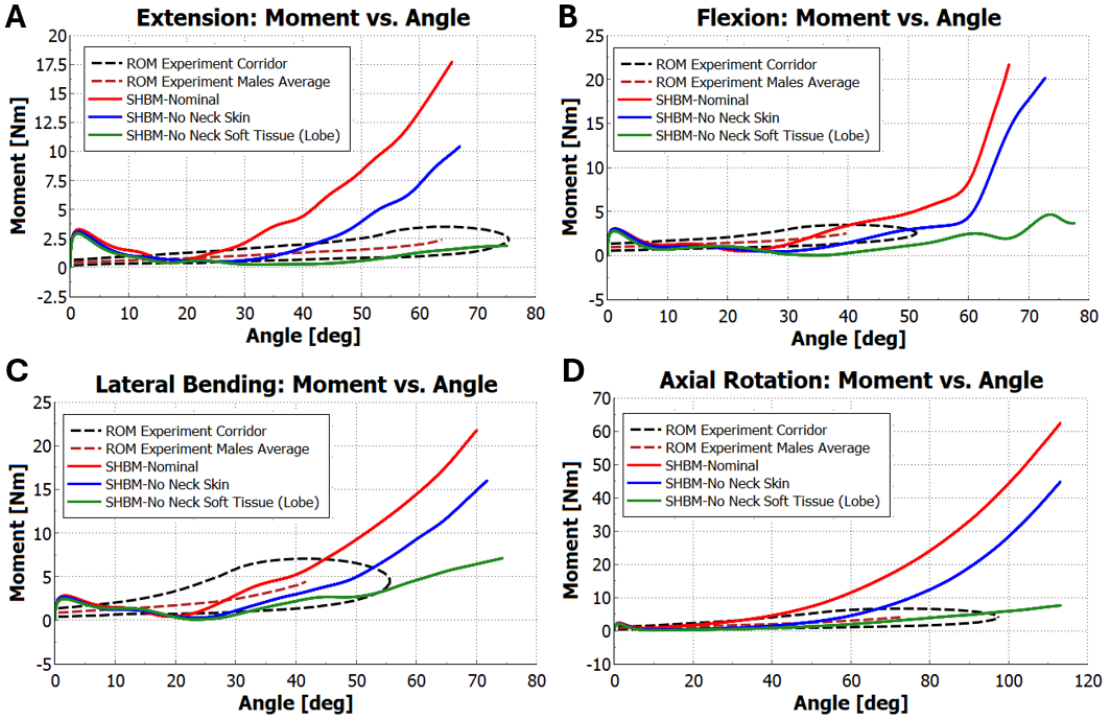

Figure 9: Neck soft tissue contribution to ROM with SHBM. A: Extension. B: Flexion. C: Left lateral bending. D: Left axial rotation.

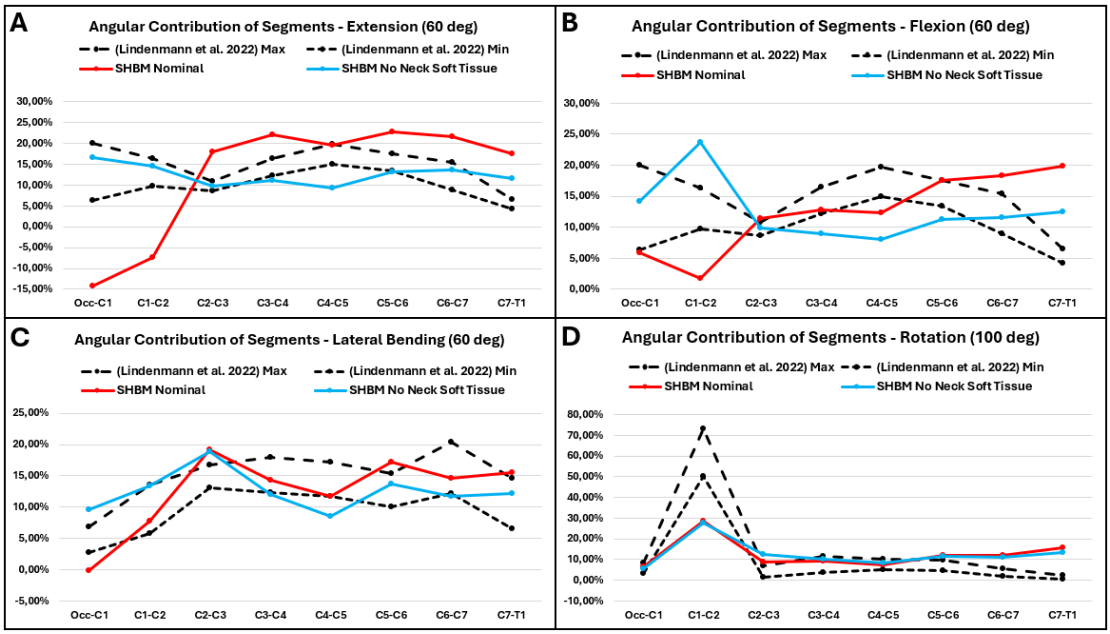

Figure 10: Comparison of segments' angular contribution with SHBM segments. A: Extension. B: Flexion. C: Lateral bending. D: Axial rotation.

5 Objective 2: Parameter Study to Investigate the Contributions of the Neck Soft Tissue Modeling to ROM Results

According to the findings obtained in Objective 1, the SHBM exhibits a stiffer neck compared to the ROM experiment males average. This increased stiffness was primarily attributed to the neck lobe components of the SHBM. To address this challenge, Objective-2 described in section 1.1 was implemented.

5.1 Methodology

Within this objective, the material properties of the SHBM's neck skin and neck flesh were investigated. In each simulation trial, only one parameter of a single component was altered to isolate and understand its individual effect on neck moment vs angle values.

In the following phase, promising material configurations identified in earlier stages for each part (neck skin and neck flesh) were combined. This approach aimed to achieve a model in which the contributions of both the neck skin and the neck flesh to overall neck moment vs angle values were effectively reduced.

5.1.1 Neck skin parameter study

Since the neck skin exhibits a viscoelastic behavior (Ottenio et al. 2015), it was essential to utilize material models capable of capturing this characteristic. In the current version of SHBM (v11.1.0), the neck skin is modeled by using `MAT_034: FABRIC` with two material curves determining stress vs strain response in two different directions (see Figure 11), to model the bi-directional properties of human skin. In the conducted parameter studies, two material types were considered to represent the viscoelastic nature of the skin: `MAT_034: FABRIC` and `MAT_077_O: OGDEN_RUBBER`.

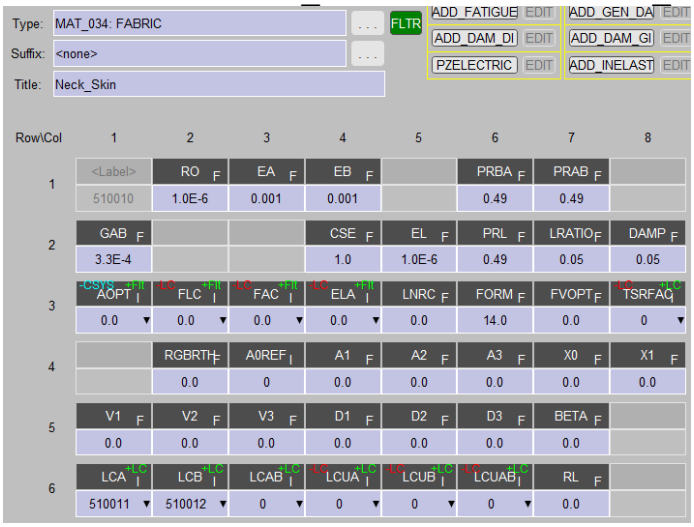

Figure 11: SHBM neck skin material card.

In the first approach, the goal was to soften the existing material by adjusting parameters within the same material card. The underlying hypothesis was that the human neck skin may be slack in its neutral, unloaded state. Therefore, the stress-strain response used in SHBM might cause the neck skin to become stiff earlier than it would in reality. To address this, the stress-strain curve was shifted horizontally along the

strain (x) axis in a positive direction as it is shown in the Figure 12. This approach maintains lower stress levels up to a certain strain threshold, corresponding to the estimated neutral position of the skin, thus yielding a softer material response. In this trial, the stress-strain curve was shifted from the 0% strain point to the approx. 40% strain point (see Figure 12 and Table 2), and the simulation was executed with this modified configuration. In another trial, the simulation was conducted with modified Young's modulus and Shear modulus values (see Table 2).

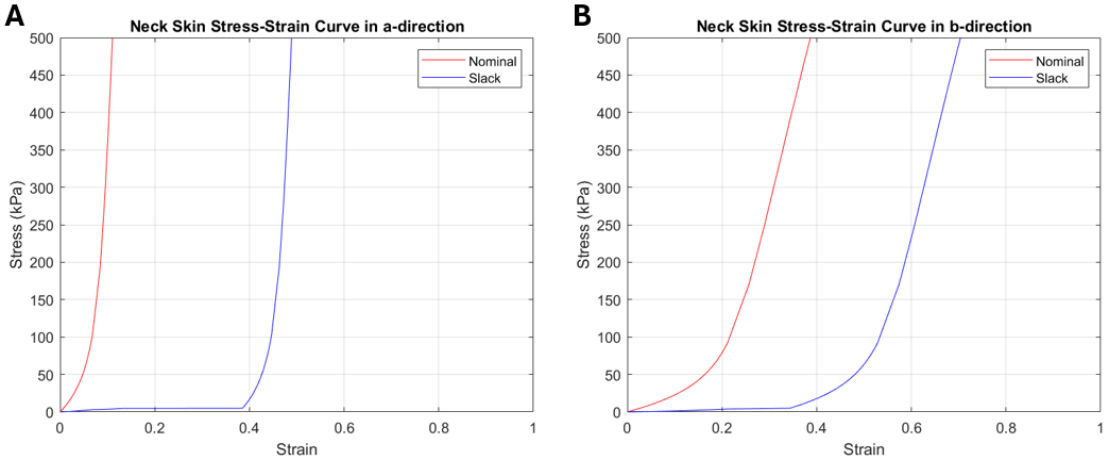

Figure 12: SHBM neck skin stress-strain curves. A: In a-direction (parallel to Langer's line). B: In b-direction (perpendicular to Langer's line).

Shifting the stress-strain curve of the skin material can reduce its stiffness and make the neck softer. However, human skin exhibits different mechanical responses depending on the strain rate. Therefore, this approach may result in the skin remaining too soft during movements involving accelerations higher than the ROM. To address this issue, a strain-rate-dependent material model may be useful. For this purpose, tables describing stress–strain results vs. various strain rates, listed in Figure 13, were created using different curves for different strain rates and were applied to the SHBM skin material model. The curves used in the tables are the scaled versions of the curves used in the SHBM nominal version as they are shown in Figure 13.

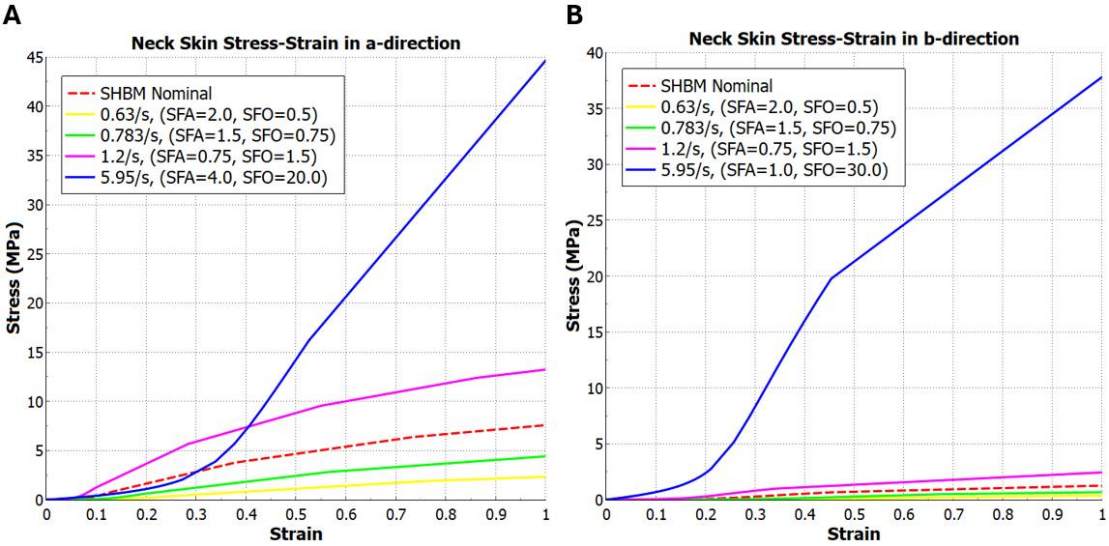

Figure 13: Strain-rate dependent neck skin. A: In a-direction (parallel to Langer's line). B: In b-direction (perpendicular to Langer's line), (SFA: Scale Factor for Abscissa, SFO: Scale Factor for Ordinate).

In the second approach, a neck skin material card recently developed (Panzer et al. 2024) was implemented in SHBM. A total of two simulations were run with this material card with different element formulations, see Table 2.

All parameter studies conducted for the SHBM neck skin are then summarized in the Table 2. The neck moment results then were compared with the ROM experiment males average neck moment results at the average maximum angular rotation, and nominal SHBM neck moments in Table 5.

Table 2: Parameter study for SHBM neck skin material.

Trial No	Material Title	Material Type	Description	Simulation Status
1	SHBM Neck Skin	MAT_034: FABRIC	Stress-strain curves were shifted	COMPLETED
2	SHBM Neck Skin	MAT_034: FABRIC	Young's modulus (EA, EB, EL) and shear modulus (GAB) values were halved	COMPLETED
3	SHBM Neck Skin	MAT_034: FABRIC	Stress-strain tables, for different strain rates, were created	COMPLETED
4	(Panzer et al. 2024) Material Model of Skin	MAT_077_O: OGDEN_RUBBER	Default values were used (SHBM's current element properties)	FAILED
5	(Panzer et al. 2024) Material Model of Skin	MAT_077_O: OGDEN_RUBBER	Element Formulation was selected as "25"	COMPLETED

5.1.2 Neck flesh parameter study

Based on the findings from Objective 1, the neck muscle properties in SHBM appear to be represented both by the muscle beams and the neck flesh. This likely results in a duplication of muscle characteristics in the model, which may account for the observed high neck moment values. To address this issue, a parameter study was conducted focusing on the material properties of the neck flesh (the solid elements in the neck lobe). This involved modifying the existing neck flesh material card used in SHBM (see Figure 14), as well as testing alternative materials that could provide the desired level of softness.

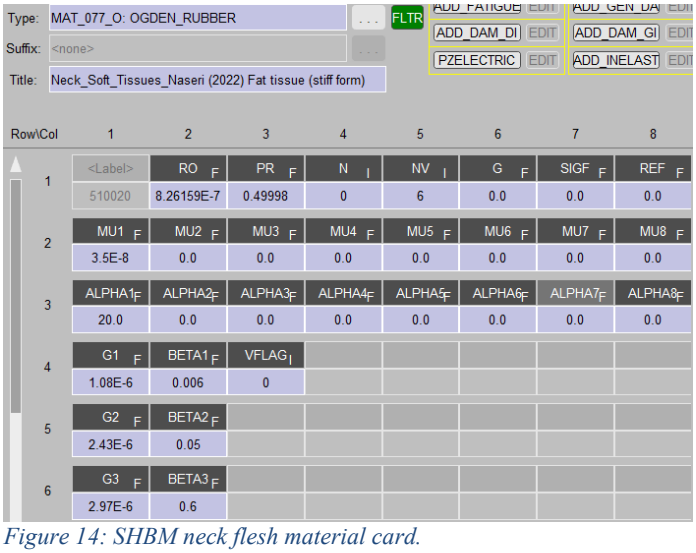

Figure 14: SHBM neck flesh material card.

Hyperelastic material models were selected, as the human neck consists of biological tissues that exhibit nonlinear and viscoelastic behavior (Cronin et al. 2018). While aiming to reduce neck moment values through these material changes, care was also taken to ensure stability of simulation. Consequently, in some cases, multiple simulations were performed using the same material type to achieve a successful run.

The parameter study included biological material models such as adipose and muscle tissues (Naseri 2022; Panzer et al. 2024). In addition to these, several trials were conducted using industrial materials, such as foam and rubber, to achieve a sufficiently soft neck flesh model, thereby avoiding the duplication of muscle properties already represented by the beams in the model. Specifically, cushion foams (models derived from a seat cushion foam model available in the Autoliv repository) and solid silicone rubber (Yamashita et al. 2023) were tested as alternative neck flesh materials. In total, 17 simulation trials were carried out and summarized in Table 3.

Table 3: Parameter study for SHBM neck flesh material.

Trial No	Material Title	Material Type	Description	Simulation Status
1	(Naseri 2022) Soft Material Model of Adipose	MAT_077_O: OGDEN_RUBBER	Default values were used (SHBM's current element properties)	COMPLETED
2	(Naseri 2022) Soft Material Model of Adipose	MAT_077_O: OGDEN_RUBBER	The Poisson's ratio (Pr) decreased from 0.498 to 0.49	COMPLETED
3	(Naseri 2022) Soft Material Model of Adipose	MAT_077_O: OGDEN_RUBBER	The Poisson's ratio decreased from 0.498 to 0.45 (compressible)	COMPLETED
4	(Naseri 2022) Soft Material Model of Adipose	MAT_077_O: OGDEN_RUBBER	The Shear modulus (Mu) decreased from 3.5E-8 to 3.0E-8	COMPLETED
5	(Naseri 2022) Soft Material Model of Adipose	MAT_077_O: OGDEN_RUBBER	-The Poisson's ratio (Pr) decreased from 0.498 to 0.49 - The Shear modulus (Mu) decreased from 3.5E-8 to 3.0E-8	COMPLETED
6	(Naseri 2022) Alternative Material Model of Adipose	MAT_077_O: OGDEN_RUBBER	Default values were used (SHBM's current element properties)	COMPLETED
7	(Panzer et al. 2024) Material Model of Adipose	MAT_077_O: OGDEN_RUBBER	Default values were used (SHBM's current element properties)	FAILED

8	(Panzer et al. 2024) Material Model of Adipose	MAT_077_O: OGDEN_RUBBER	Element Formulation was selected as “5”	FAILED
9	(Panzer et al. 2024) Material Model of Adipose	MAT_077_O: OGDEN_RUBBER	New Hourglass was created with HIQ=5	FAILED
10	(Panzer et al. 2024) Material Model of Muscle	MAT_077_O: OGDEN_RUBBER	Default values were used (SHBM’s current element properties)	FAILED
11	(Panzer et al. 2024) Material Model of Muscle	MAT_077_O: OGDEN_RUBBER	Hourglass was selected as “Stiffness based HG solids HIQ=5”	COMPLETED
12	(Panzer et al. 2024) Material Model of Muscle	MAT_077_O: OGDEN_RUBBER	Hourglass, created on the 8th trial, was selected	COMPLETED
13	Solid Silicone Rubber Material Model	MAT_077_O: OGDEN_RUBBER	New material card was created based on (Yamashita et al. 2023)	COMPLETED
14	Cushion Foam Model	MAT_057: LOW_DENSITY_ FOAM	New material card was created by using the seat cushion foam material model	COMPLETED
15	Cushion Foam Model	MAT_057: LOW_DENSITY_ FOAM	-Young’s modulus decreased from 2.76E-4 to 2.0E-5 -Damping coefficient increased from 0.02 to 0.03 -Stress-strain curve scaled as “SFA=5.0, SFO=0.2”	COMPLETED
16	Cushion Foam Model	MAT_057: LOW_DENSITY_ FOAM	-Young’s modulus decreased from 2.76E-4 to 1.5E-5 -Damping coefficient increased from 0.02 to 0.03 -Stress-strain curve scaled as “SFA=10.0, SFO=0.1”	COMPLETED

17	Cushion Foam Model	MAT_057: LOW_DENSITY_FOAM	-Young's modulus decreased from 2.76E-4 to 5.2E-5 -Damping coefficient increased from 0.02 to 0.03 -Stress-strain curve scaled as "SFA=5.0, SFO=0.2"	COMPLETED

The neck moment results of these trials were compared in Table 6 with nominal SHBM and ROM experiment males average results at the maximum angular rotation.

5.1.3 Overall neck (neck lobe) parameter study

In the final phase of the parameter study, configurations that effectively reduced neck moment values were combined for both the neck skin and the neck flesh. This strategy aims to decrease overall neck moment values by simultaneously softening both components. In these combinations, some trials that make the model unstable are not included. The tested combinations are summarized in Table 4.

Table 4: Parameter study for the SHBM overall neck soft tissue (neck lobe).

Combination No	Neck Skin Material Model	Neck Flesh Material Model	Simulation Status
1	SHBM Neck Skin / Trial No: 1	(Naseri 2022) Soft Material Model of Adipose / Trial No: 2	COMPLETED
2	SHBM Neck Skin / Trial No: 1	(Naseri 2022) Soft Material Model of Adipose / Trial No: 5	COMPLETED
3	SHBM Neck Skin / Trial No: 3	(Naseri 2022) Soft Material Model of Adipose / Trial No: 2	COMPLETED
4	SHBM Neck Skin / Trial No: 3	Cushion Foam Model / Trial No: 15	FAILED
5	SHBM Neck Skin / Trial No: 3	Cushion Foam Model / Trial No: 16	FAILED
6	SHBM Neck Skin / Trial No: 3	Cushion Foam Model / Trial No: 17	COMPLETED

Then, the neck moment results of these combinations were compared in Table 7 with nominal SHBM and ROM experiment males average results at the maximum angular rotation. Also, the angular contribution of the segments was compared between the nominal SHBM, SHBM without neck lobe and SHBM with updated parameters (only the most promising one).

5.2 Results

Following the completion of the parameter studies, the neck moment vs angle measurements were compared against the results obtained from the SHBM Nominal and ROM experiments. It should be noted that the results of the failed simulations, where error termination occurred due to instability issues, were excluded from these comparisons.

5.2.1 Neck skin parameter study

The influence of the parameter variations applied to the SHBM neck skin on neck moment values is summarized in Table 5 for each trial. A reduction in neck moment was observed in the trials involving slack skin and strain-rate dependent skin models as they are shown in Figure 15. However, halving the Young's modulus and the shear modulus did not reduce the neck moment. The trial (Trial No: 5) employing the skin model proposed by (Panzer et al. 2024) resulted in an increase in neck moment (see Appendix Figure A 1).

Table 5: Neck moment results at the males average maximum ROM angle for parameter study of SHBM neck skin.

	Extension (64 deg)	Flexion (40 deg)	Lateral Bending (42 deg)	Axial Rotation (72 deg)
ROM Experiment Males Average	2.41 Nm	2.49 Nm	4.42 Nm	4.04 Nm
SHBM Nominal	16.46 Nm	3.41 Nm	5.86 Nm	18.27 Nm
Trial No: 1	12.89 Nm	1.80 Nm	4.03 Nm	13.43 Nm
Trial No: 2	16.40 Nm	3.45 Nm	5.86 Nm	16.47 Nm
Trial No: 3	10.25 Nm	1.72 Nm	3.60 Nm	12.75 Nm
Trial No: 4	-	-	-	-
Trial No: 5	31.06 Nm	5.66 Nm	10.89 Nm	49.59 Nm

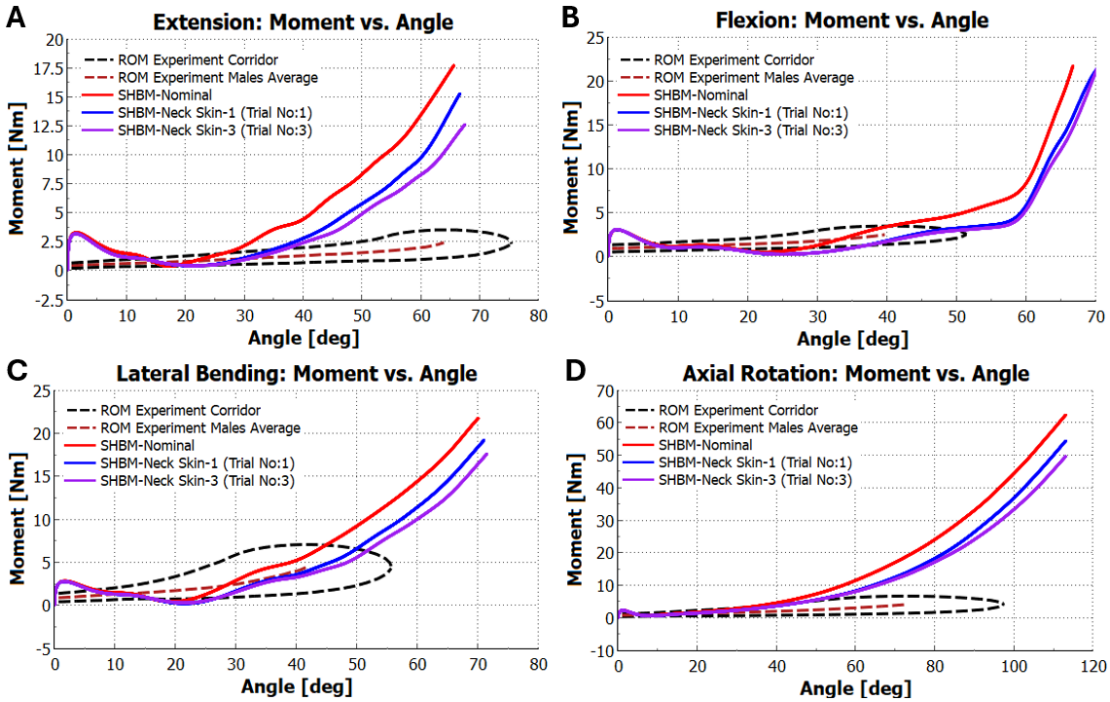

Figure 15: Moment vs. angle results for modified SHBM neck skin material. A: Extension. B: Flexion. C: Left lateral bending. D: Left axial rotation.

5.2.2 Neck flesh parameter study

The effects of the parameter studies conducted on SHBM neck flesh with respect to neck moment values are presented in Table 6 for each trial. Simulations that failed were omitted from the analysis. In addition to this, the solid silicone rubber model (Trial No: 13) was also excluded due to the material card not functioning.

Some of the trials that provided significant reduction in neck moment were selected and their comparison with SHBM Nominal and ROM test results are given in Figure 16

(see Appendix Figure A 2 and Figure A 3 for the trials that did not provide neck moment reduction).

Table 6: Neck moment results at the males average maximum ROM angle for parameter study of SHBM neck flesh.

	Extension (64 deg)	Flexion (40 deg)	Lateral Bending (42 deg)	Axial Rotation (72 deg)
ROM Experiment Males Average	2.41 Nm	2.49 Nm	4.42 Nm	4.04 Nm
SHBM Nominal	16.46 Nm	3.41 Nm	5.86 Nm	18.27 Nm
Trial No: 1	13.93 Nm	3.22 Nm	5.57 Nm	17.30 Nm
Trial No: 2	12.40 Nm	3.05 Nm	5.37 Nm	16.45 Nm
Trial No: 3	11.70 Nm	2.84 Nm	5.25 Nm	15.91 Nm
Trial No: 4	13.56 Nm	3.14 Nm	5.52 Nm	16.90 Nm
Trial No: 5	12.20 Nm	2.98 Nm	5.34 Nm	16.09 Nm
Trial No: 6	16.65 Nm	3.49 Nm	6.00 Nm	19.54 Nm
Trial No: 7	-	-	-	-
Trial No: 8	-	-	-	-
Trial No: 9	-	-	-	-
Trial No: 10	-	-	-	-
Trial No: 11	20.93 Nm	4.14 Nm	8.49 Nm	20.03 Nm
Trial No: 12	20.93 Nm	4.14 Nm	8.49 Nm	20.03 Nm
Trial No: 13	-	-	-	-
Trial No: 14	23.08 Nm	7.09 Nm	10.73 Nm	25.80 Nm
Trial No: 15	11.77 Nm	3.18 Nm	5.22 Nm	12.72 Nm
Trial No: 16	11.44 Nm	2.90 Nm	5.07 Nm	12.18 Nm
Trial No: 17	13.26 Nm	3.71 Nm	5.94 Nm	14.21 Nm

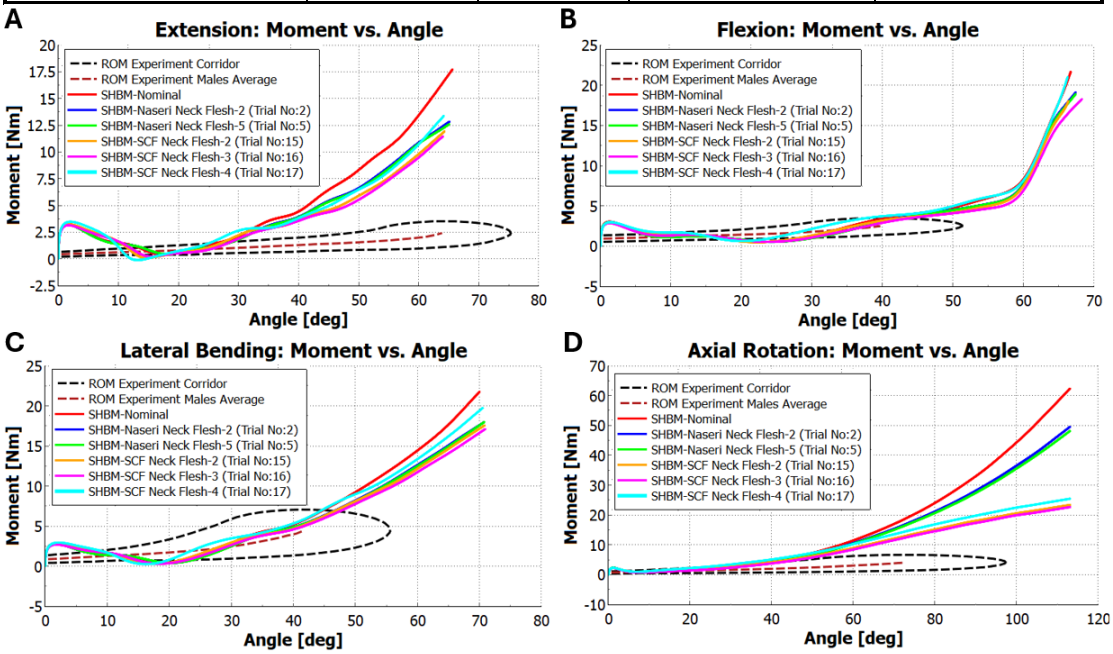

Figure 16: Modified SHBM neck flesh parameters that reduce neck moment. A: Extension. B: Flexion. C: Left lateral bending. D: Left axial rotation.

5.2.3 Neck lobe parameter study

In this section, the neck moment values results obtained from the neck lobe parameter study are shown for each combination in Table 7. The results of failed simulations are excluded.

A comparison of the simulation results with both the ROM experiment data and SHBM nominal values is presented in Figure 17. The results indicate that all tested combinations led to a reduction in neck moment relative to the SHBM nominal model. Notably, stiffness values approximating those of the ROM experiment males average were achieved in extension and axial rotation. In contrast, the moment values observed during flexion and lateral bending were lower than those of the ROM experiment males average, indicating too soft response. Among the configurations, Combination No: 6, featuring cushion foam (Trial No: 17) neck flesh and strain-rate-dependent neck skin (Trial No: 3), demonstrated effective softening in both extension and axial rotation, while also exhibiting the least deviation in flexion and lateral bending responses (see Table 7).

Further analysis of the combinations incorporating (Naseri 2022) adipose models revealed that Combination No: 3 achieved substantial softening. On the other hand, Combination No: 1 and 2 produced similar results but provided stiffer neck responses than Combination No: 3.

Table 7: Neck moment results at the males average maximum ROM angle for parameter study of SHBM neck lobe.

	Extension (64 deg)	Flexion (40 deg)	Lateral Bending (42 deg)	Axial Rotation (72 deg)
ROM Experiment Males Average	2.41 Nm	2.49 Nm	4.42 Nm	4.04 Nm
SHBM Nominal	16.46 Nm	3.41 Nm	5.86 Nm	18.27 Nm
Combination No: 1	8.82 Nm	1.22 Nm	3.56 Nm	11.43 Nm
Combination No: 2	8.62 Nm	1.15 Nm	3.52 Nm	11.10 Nm
Combination No: 3	4.58 Nm	1.13 Nm	3.09 Nm	9.92 Nm
Combination No: 4	-	-	-	-
Combination No: 5	-	-	-	-
Combination No: 6	5.16 Nm	2.43 Nm	3.63 Nm	7.77 Nm

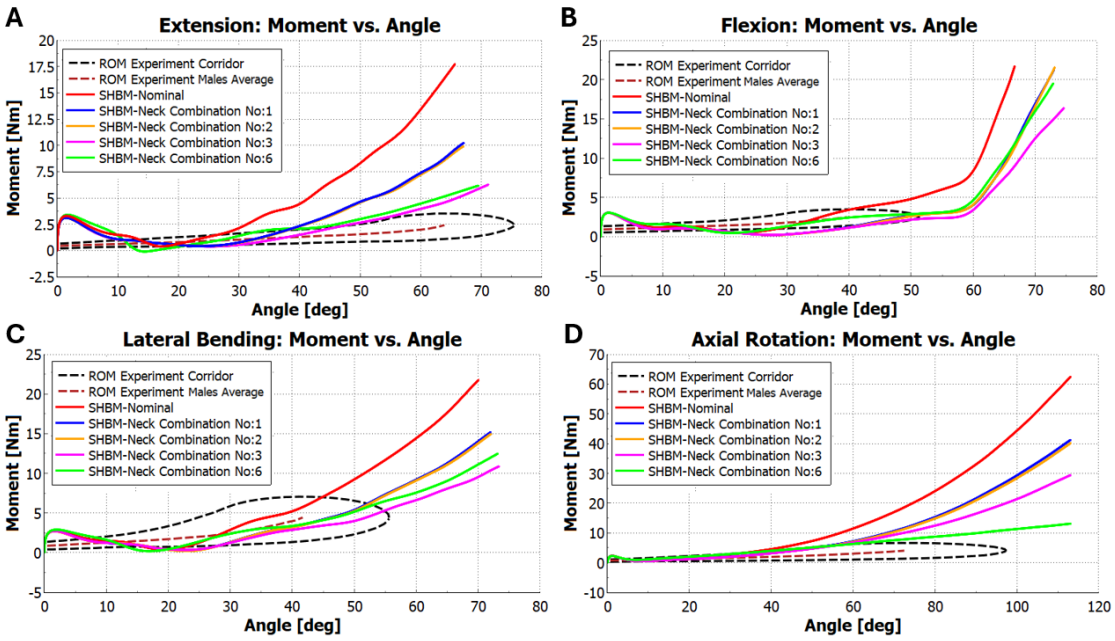

Figure 17: Modified SHBM neck lobe parameters that reduce neck moment. A: Extension. B: Flexion. C: Left lateral bending. D: Left axial rotation.

Based on the findings from the parameter study, Combination No: 1, 3, and 6 were identified as the most promising for calibration in high-acceleration motion scenarios. In addition to this, the neck skin models (see Table 2; Trial No: 1 and Trial No: 3) and neck flesh models (see Table 3; Trial No: 2 and Trial No: 17) used in these combinations were selected for use in further high-acceleration motion simulations.

The influence of the softened neck response provided by Combination No: 3, selected as the more reliable parameter combination, on the angular contributions of segments was analyzed, as illustrated in Figure 18. While axial rotation remained unaffected, a reduction in the influence of neck soft tissues was observed in lateral bending and flexion, yielding results more closely aligned with those of the model excluding neck soft tissue components. The most notable improvement was seen in extension, where unintended segmental rotations, particularly between Occ–C1 and C1–C2, were substantially mitigated and more closely matched experimental measurements (Lindenmann et al. 2022).

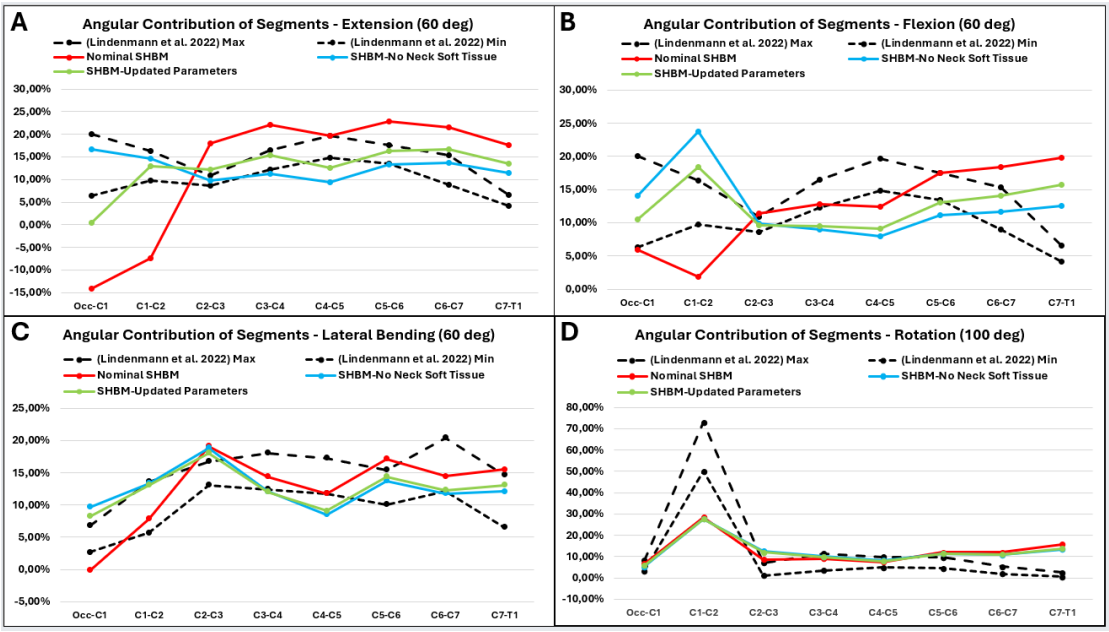

Figure 18: Effect of using updated parameters (Neck Combination No: 3) in angular contribution of segments. A: Extension. B: Flexion. C: Lateral bending. D: Axial rotation.

6 Objective-3: Evaluation and Calibration for High Acceleration Scenarios

In this thesis, the experiments on the head and neck responses of PMHSs conducted by (Kang et al. 2018) were selected to be simulated in finite element simulations for the high acceleration scenario. After the parameter study performed with ROM, the calibration for the high acceleration scenario was done with these simulations.

In these experiments (Kang et al. 2018), five PMHSs were subjected to dynamic tests for frontal, oblique, side and twist scenarios by attaching them to the mini-sled system. In these tests, body parts consisting of the head, neck, and lower neck soft tissues (the soft tissues between the neck and upper chest, excluding internal organs) of PMHS were used in the bending tests. In the twist test, a PMHS consisting of only the head and neck was used. The mini-sled velocity was set as 14 km/h for frontal, side and oblique tests and 1800 deg/s for the twist test. In this way, the biomechanical responses of the head and lower neck were measured under various impact conditions.

In this study, oblique and twist scenarios were simulated with FE modeling using SHBM. Trials and combinations that contributed to reducing neck moment values in the parameter study in Objective-2 were selected for these simulations. In this way, the results obtained from the parameter study were evaluated and calibrated for high-acceleration motion.

6.1 Methodology

To replicate the oblique and twist tests conducted by (Kang et al. 2018), two distinct sectional models of the SHBM were developed using the boundary condition models from Chalmers Validation Repository, previously developed for SHBM V.11.0. These were updated for SHBM V11.1.1. used in this thesis. For the oblique impact simulations, a sectioned model comprising the head, neck, upper thorax soft tissues, and vertebrae from C1 down to T3 was extracted, as shown in Figure 19A. For the twist simulations, a model including the head, neck, and vertebrae from C1 down to T1 was used, as shown in Figure 19B. This approach enabled the creation of simplified models closely resembling the PMHS configurations used in the tests.

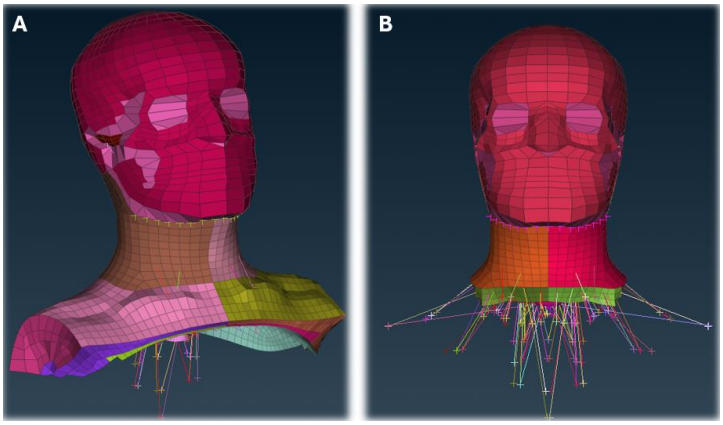

Figure 19: SHBM sections for Kang simulations. A: Oblique model. B: Twist model.

The lower neck moments obtained from the simulations were first compared with the nominal SHBM, SHBM without neck lobe and PMHS results. Then, the neck skin and

neck flesh trials, and neck lobe combinations selected in Objective-2 were evaluated in Kang simulations. The lower neck moment results were compared with the nominal SHBM and PMHS results.

6.1.1 Boundary conditions and simulation set-up for oblique scenario

To simulate the oblique scenario using the SHBM, a pot and an elliptical ring were used, following the setup used in the PMHS tests. The T3 vertebra was constrained to the pot to fix the vertebral column, while the thoracic soft tissue was constrained to the elliptical ring. A sled model was then designed to replicate the acceleration profile used in the physical tests.

At the beginning of the physical PMHS tests, the head was supported by a harness and gently released under the effect of gravity. Immediately prior to the onset of sled motion, the harness released the head completely. To replicate this behavior in the simulation, the SHBM's head was initially supported using a repositioning beam element with constant stiffness. The model was then subjected to gravity loading to mimic a natural resting posture. This positioning phase lasted for the first 300 milliseconds of the simulation. At the 300 ms mark, the repositioning beam constraint was removed, allowing the SHBM head to move freely.

Once the SHBM stabilized under gravity by 300 ms (see Figure 20), a prescribed acceleration was applied in the horizontal (xy) plane to the sled, whose movement was constrained in the vertical (z) axis, to simulate the oblique impact. In the physical tests, the elliptical ring was mounted to the mini-sled, allowing the applied motion to be transmitted to the PMHS. To replicate this configuration, the same boundary conditions applied to the sled were also applied to the elliptical ring. Furthermore, to ensure motion transfer to the vertebral column, the pot to which the T3 vertebra was attached was rigidly constrained to the sled.

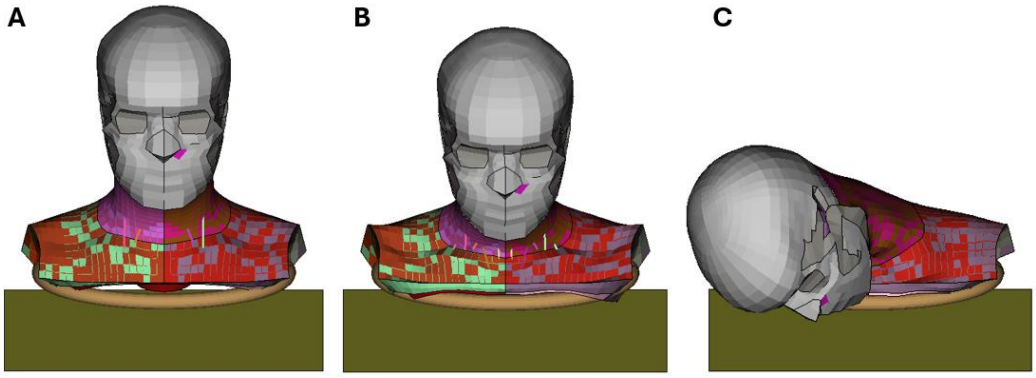

Figure 20: Oblique simulation with SHBM. A: Initial step. B: At 300th ms. C: At 390th ms.

For the oblique simulations, the trials and combinations specified in Objective-2 (see Section 5.2.3) were executed using 16 MPP processors, with a total termination time of 550 ms.

6.1.2 Boundary conditions and simulation set-up for twist scenario

A similar setup to that used in the oblique scenario was implemented for the twist simulations. However, in contrast to the oblique case, the T2 and T3 vertebrae were removed in the PMHSs tests, and thus the T1 vertebra was attached to the pot. Additionally, instead of the upper thorax soft tissue, the neck soft tissue was connected to the elliptical ring. In this configuration, a head holder was used to stabilize the head.

To replicate the twist scenario with the SHBM, an elliptical ring, a pot, and a sled were modeled. The SHBM's neck soft tissue was constrained to the elliptical ring, the T1 vertebra to the pot, and the pot was rigidly constrained to the sled. Unlike the oblique scenario, where linear acceleration was applied, rotational motion was simulated by prescribed rotational velocity about the vertical (z) axis to the sled.

Throughout the twist test, the PMHS head was held stationary using mechanical holders. To replicate this condition, two head holders were modeled to fix the SHBM's head. These holders were engaged at the beginning of the simulation and remained clamped to the head for its entire duration (see Figure 21).

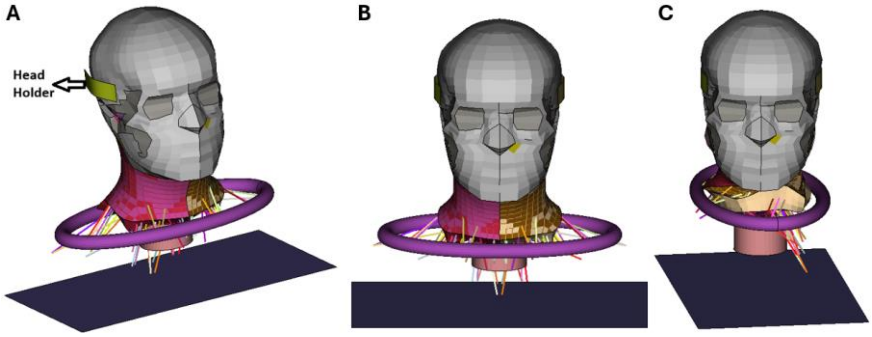

Figure 21: Twist set-up with SHBM. A: Initial step isometric view. B: Initial step front view. C: Last step front view.

The twist simulations were conducted using the trials and combinations specified in Objective-2 (see Section 5.2.3). All simulations were run using 16 MPP processors, with a total termination time of 250 milliseconds.

6.2 Results and Evaluation of Parameter Study with Kang Simulations

To visualize the movements expressed by the results, the positioning of the SHBM in the coordinate system for both the oblique and twist scenarios is depicted in Figure 22.

The simulations conducted with the nominal SHBM and the SHBM without neck lobe were compared against the PMHS test results for the lower neck moments under the twist scenario, as shown in Figure 23B. Additionally, the angular rotation vs. time curve applied as input to the sled disk in twist simulations is also shown in Figure 23A. In this case, the initial 50 ms when the head holders were attached were omitted, and the 50th ms was considered the starting point (0 ms).

Head rotations and lower neck moments, across all three axes (x-y-z) under the oblique loading scenario were compared against PMHSs test results as illustrated in Figure 24. The initial 300 ms corresponding to the positioning phase of the SHBM were excluded from the simulation data, and the 300th millisecond was considered the starting point of the experiment (0 ms). Furthermore, since PMHSs test data extended only up to 200 ms, the final 50 ms of the simulation results were also omitted.

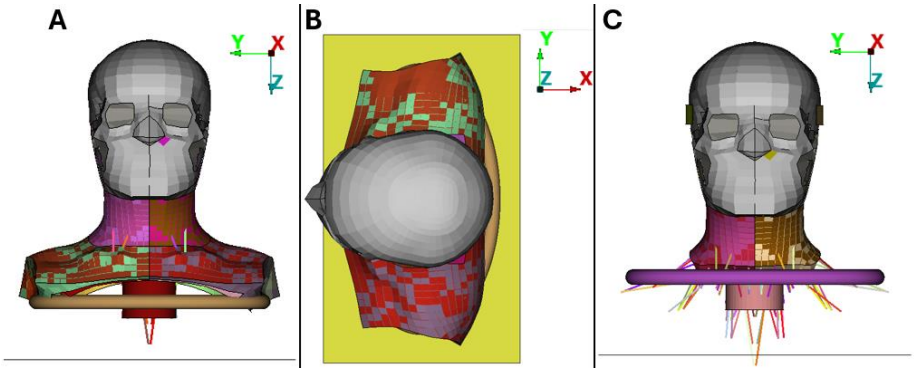

Figure 22: SHBM positioning. A: Oblique - Front view. B: Oblique - Top view. C: Twist – Front view.

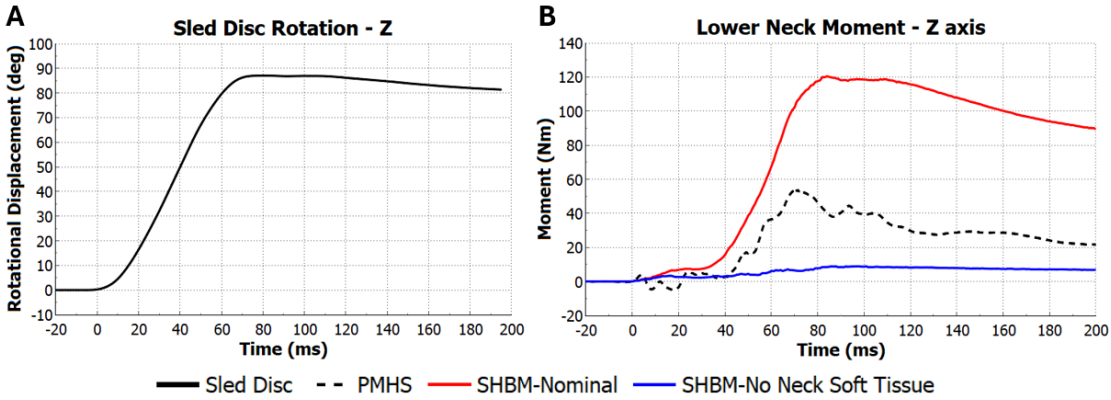

Figure 23: Twist scenario, A: Sled disc rotation about the z axis (input for twist simulations); B: Lower neck moment comparison about the z axis.

In the oblique scenario, the lower neck moments increased due to the influence of the neck lobe (see Figure 24). On the other hand, when compared SHBM results with the PMHSs test data, SHBM overall neck response seems softer x-axis (lateral bending) and y-axis (extension/flexion). In addition to this, when looked particularly after 80 ms, substantial discrepancies appeared in the SHBM responses due to the SHBM head impacting to the rigid boundary condition (the elliptical ring); this was not observed in the corresponding PMHS tests. Therefore, the time window from -20 ms to 90 ms was selected for the subsequent analyses.

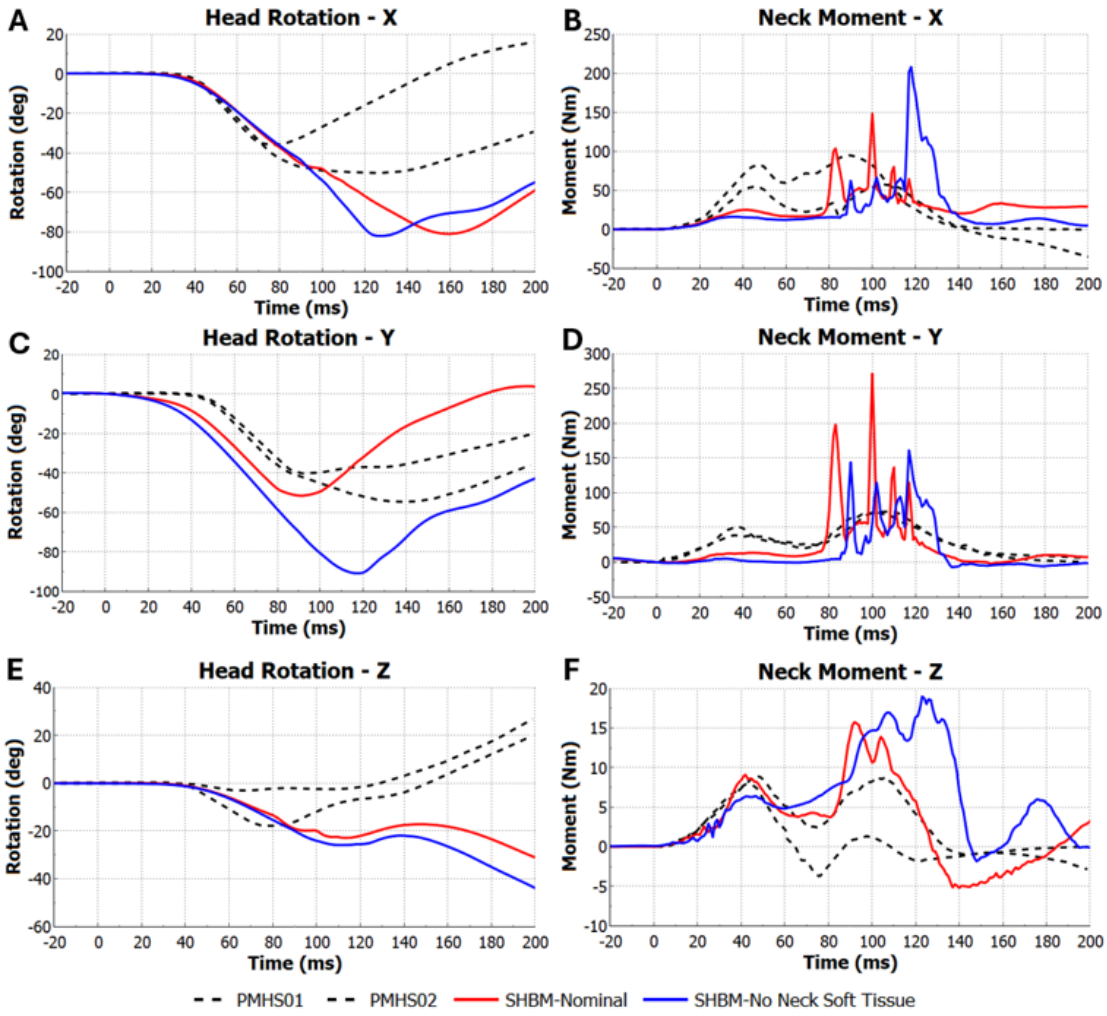

Figure 24: Head rotations comparison in oblique scenario, A: x-axis, C: y-axis, E: z-axis; and lower neck moments comparison in oblique scenario, B: x-axis, D: y-axis, F: z-axis.

6.2.1 Neck skin and neck flesh parameter study evaluation

The simulation results for the oblique scenario, based on the neck skin and neck flesh material configurations defined in Objective-2, are presented in Figure 25. The simulation using cushion foam material (Trial No: 17) for neck flesh was excluded from the analysis due to simulation failure. Examination of the results reveals that all trials produced results similar to the nominal SHBM up until the onset of rebound from head impact to the ring.

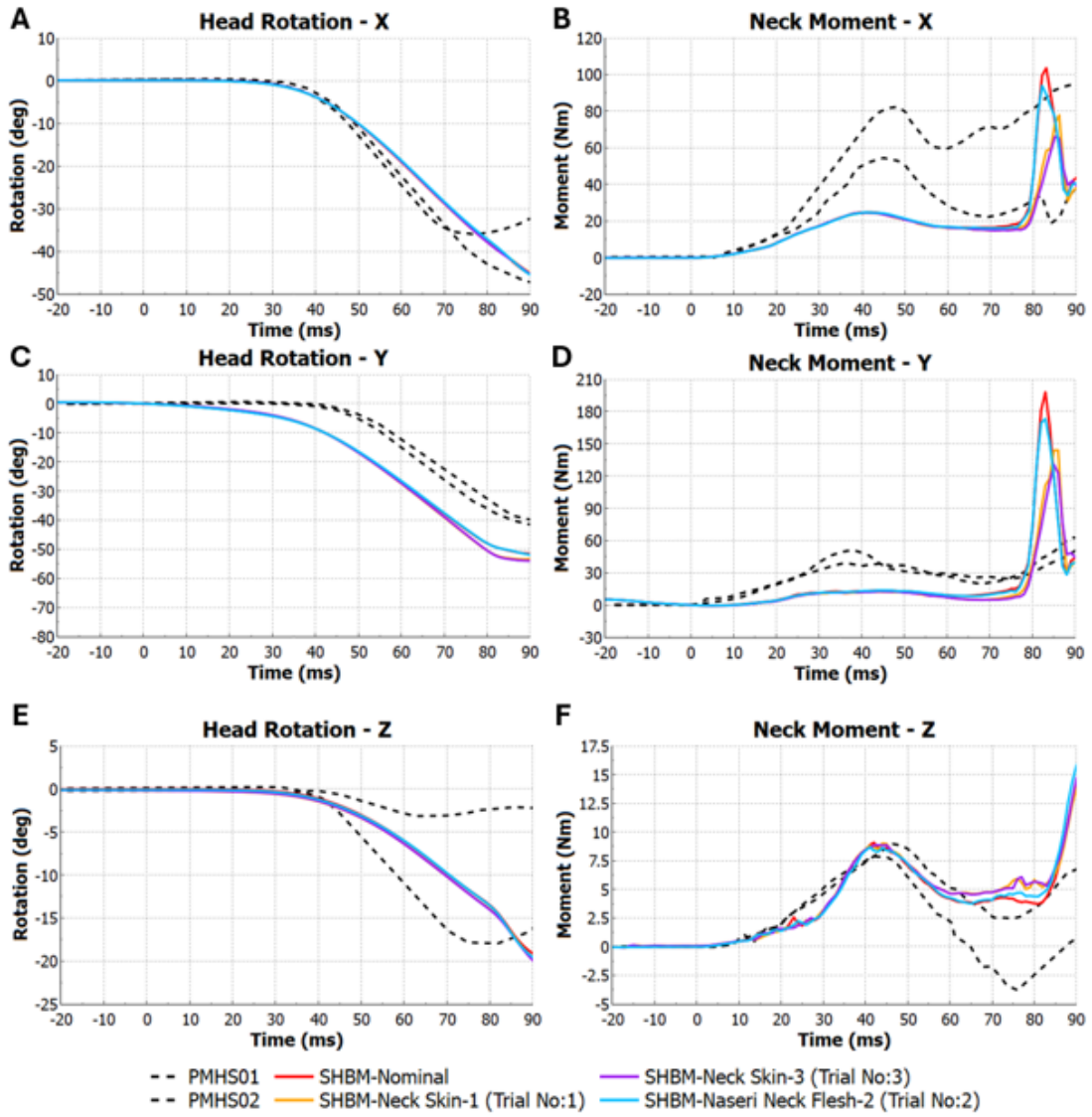

Figure 25: Effect of neck skin and neck flesh trials on head rotations comparison in oblique scenario, A: x-axis, C: y-axis, E: z-axis; and effect of neck skin and neck flesh trials on lower neck moment in oblique scenario, B: x-axis, D: y-axis, F: z-axis.

In the twist scenario, all three material configurations resulted in a reduction of the neck moment, yielding values closer to the PMHS test results (see Figure 26). However, none of the simulations fully replicated the PMHS response.

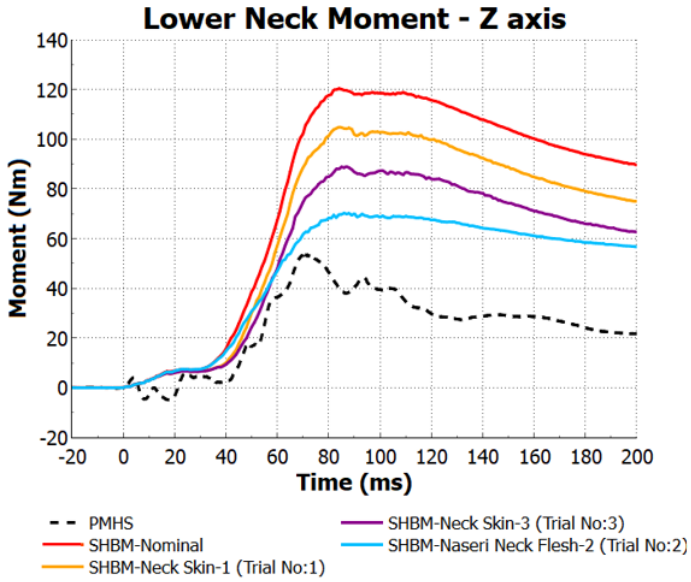

Figure 26: Effect of neck skin and neck flesh trials on lower neck moments about the z axis in twist scenario.

6.2.2 Neck lobe parameter study evaluation

In the twist scenario, both combinations resulted in a softer neck response compared to the nominal SHBM (see Figure 27). However, their overall stiffness characteristics were closer to the PMHS data, with Combination No: 3 demonstrating better alignment with the experimental results. The simulation with Combination No: 6 was excluded due to simulation failure caused by the unstable cushion foam (Trial No: 17) model.

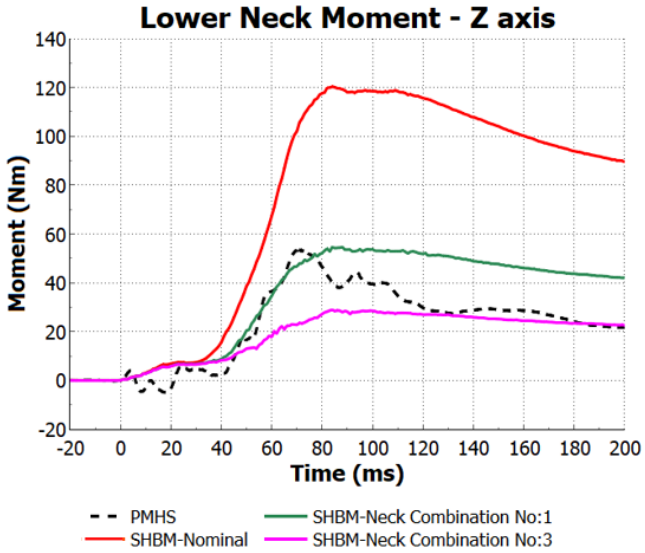

Figure 27: Effect of neck combinations on lower neck moments about the z axis in twist scenario.

The results of the oblique simulations using the neck skin and neck flesh material combinations defined in Objective-2 are presented in Figure 28. The simulation with Combination No: 6 was excluded due to simulation failure. Combination No: 1 and 3 produced responses similar to the nominal SHBM up to the onset of head contact with the ring. When compared with the PMHSs test data, both combinations continued to show a more compliant neck response than expected in the x- and y-axes.

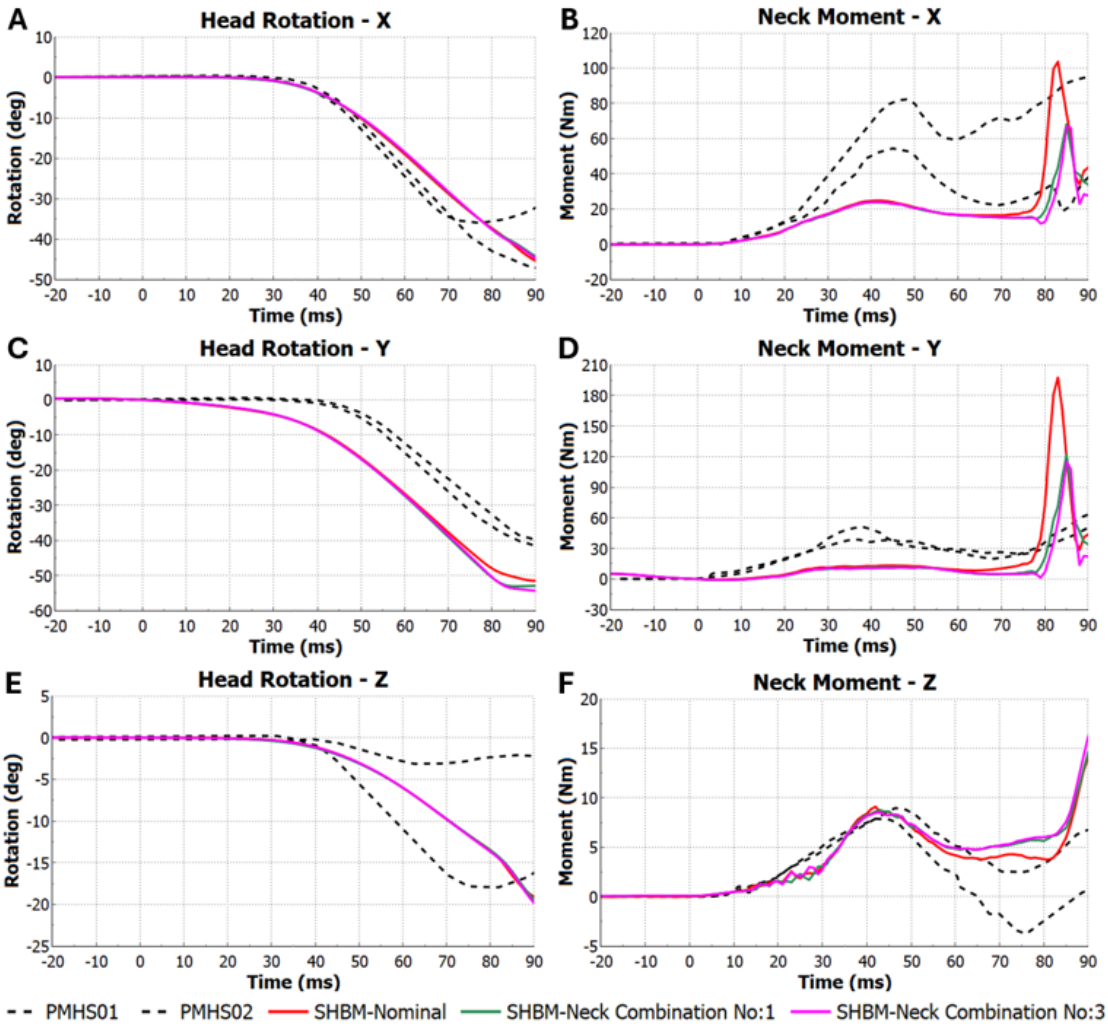

Figure 28: Effect of neck lobe combinations on head rotation in oblique scenario, A: x-axis, C: y-axis, E: z-axis; and effect of neck lobe combinations on lower neck moment in oblique scenario, B: x-axis, D: y-axis, F: z-axis.

Considering all the results, the SHBM demonstrates a softer neck response than the PMHS in extension, flexion, and lateral bending under high-acceleration impact. In axial rotation, it yields results closer to the PMHSs in the oblique scenario, whereas it exhibits a considerably stiffer response in the twist scenario.

The parameter study conducted under Objective-2 did not lead to significant improvements in the SHBM's neck response under high-acceleration conditions, except in the twist scenario.

6.3 Calibration for High Acceleration Scenarios

To calibrate the parameters for Kang simulations, modifications were implemented on the existing strain-rate dependent neck skin model (Trial No: 3). In the first step, two of the four intermediate curves in this skin model were removed. The remaining curves, corresponding to a strain rate of 5.95/s, were scaled to match the stress-strain behavior observed in tensile tests conducted on human back skin by (Ní Annaidh et al. 2012), as it is shown in Figure 29, to yield a stiffer neck response during high-acceleration movements.

On the other hand, the strain rates of the curves intended for low-acceleration motions were reduced from 0.63/s to 0.12/s. This adjustment was motivated by the observation

that 600 ms simulation end time for ROM scenarios were too short compared to the experimental durations, which ranged between 8000 and 10000 ms. Consequently, the curves corresponding to the lowest acceleration levels were revised to better represent slower motions.

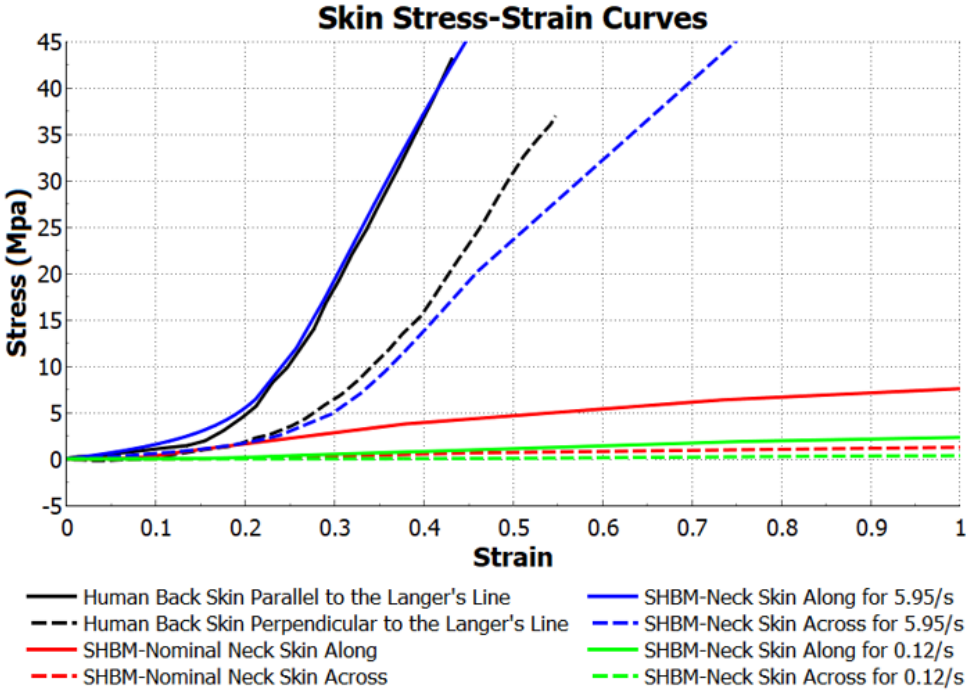

Figure 29: Skin stress-strain curves.(Along: Parallel to the Langer's Line; Across: Perpendicular to the Langer's Line)

Following these modifications (see Table 8), simulations were carried out using the newly developed neck skin model Trial No: 6 and its combination (Combination No:7) with the most optimal neck flesh model Trial No: 2.

Table 8: Modifications for high acceleration scenarios calibration.

Trial No	Material Title	Material Type	Description	Simulation Status
6 (New)	SHBM Neck Skin	MAT_034: FABRIC	Stress-strain tables were created based on Trial No: 3	COMPLETED

Combination No	Neck Skin Material Model	Neck Flesh Material Model	Simulation Status
7 (New)	SHBM Neck Skin / Trial No: 6	(Naseri 2022) Soft Material Model of Adipose / Trial No: 2	COMPLETED

6.4 Calibration Results and Discussion

No changes were observed in the Kang simulation results following the calibration; the outputs remained identical to those of the reference parameters (Trial No: 3 and Combination No: 3). Likewise, the ROM simulations yielded results consistent with the reference parameters (see Appendix Figure A 4). The angular contribution of the segments was also the same. However, as the stress-strain curve proportional to the maximum strain rate was based on a more reliable reference (Ní Annaidh et al. 2012), Combination No: 7 was selected as most promising parameters (see Appendix Figure A 5 for 2000ms ROM simulations) and to use in the validation simulations.

7 Objective-4 Updating the Model Geometry

In this section, a design update was implemented to reduce the influence of neck soft tissues on the neck responses within the ROM and to achieve a more anatomically accurate neck model.

7.1 Methodology

As part of this update, the meshes of the neck skin and neck flesh were refined, as illustrated in Figure 30. Additionally, the gap between the neck lobe and the cervical vertebrae was reduced to improve anatomical accuracy (see Figure 31). The muscle beams in the neck were also connected to the newly modeled neck flesh at the same points where they were connected in the nominal model.

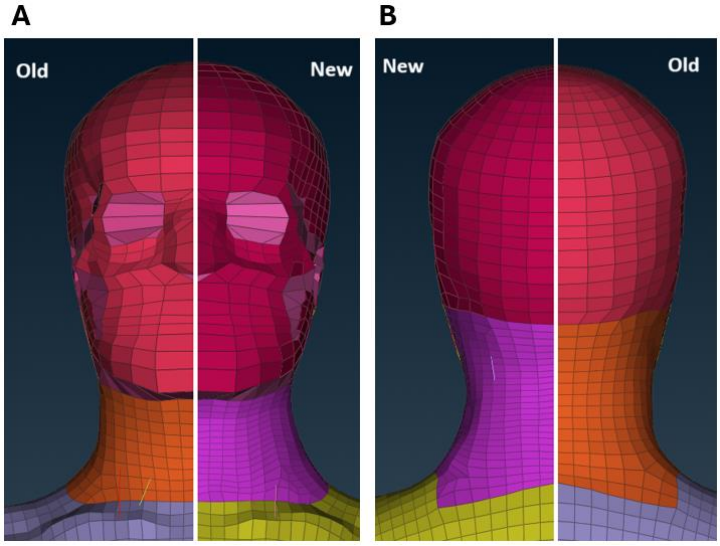

Figure 30: Mesh refinement of SHBM neck lobe. A: Front view. B: Rear view.

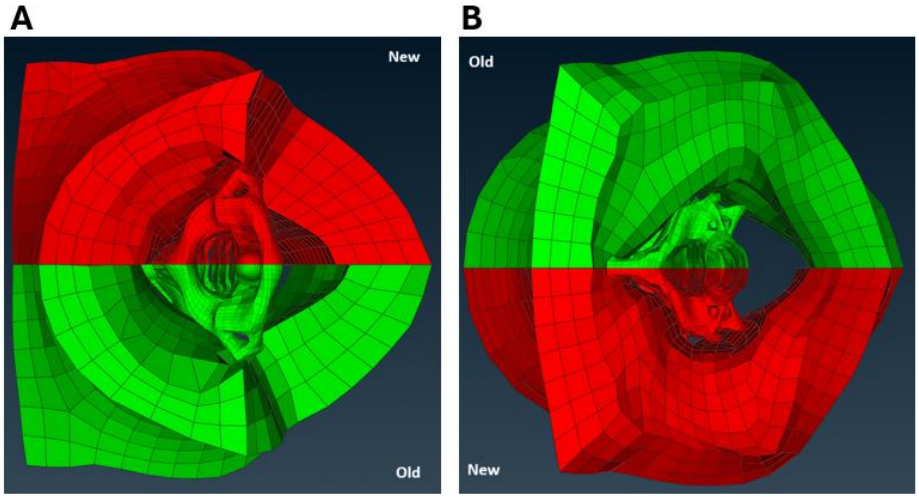

Figure 31: The gap reduction between cervical vertebrae and neck flesh. A: Top view. B: Bottom view.

In the current SHBM configuration, the cervical intervertebral ligaments are represented using beam elements, whereas the nuchal ligament is not included in the model. To improve anatomical accuracy, the nuchal ligament was modeled using shell elements, as shown in Figure 32. This structure was meshed to (i.e. shares nodes with) the neck flesh and connects the cervical vertebrae to the skull. The material type used for this structure is `MAT_034: FABRIC`, by implementing the parameters based on (Chazal et al. 1985) as illustrated in Figure 33 (see Appendix Figure A 6 for stress-

strain curves of the nuchal ligament)No changes were observed in the Kang simulation results following the calibration; the outputs remained identical to those of the reference parameters (Trial No: 3 and Combination No: 3). Likewise, the ROM simulations yielded results consistent with the reference parameters (see Appendix Figure A 4). The angular contribution of the segments was also the same. However, as the stress-strain curve proportional to the maximum strain rate was based on a more reliable reference (Ní Annaidh et al. 2012), Combination No: 7 was selected as most promising parameters (see Appendix Figure A 5 for 2000ms ROM simulations) and to use in the validation simulations..

Using the updated model, two initial ROM simulations were conducted utilizing 32 MPP processors: (1) one excluding the nuchal ligament to evaluate the effects of mesh refinement in the neck lobe; and (2) one including the nuchal ligament to assess its specific contribution to the overall biomechanical behavior.

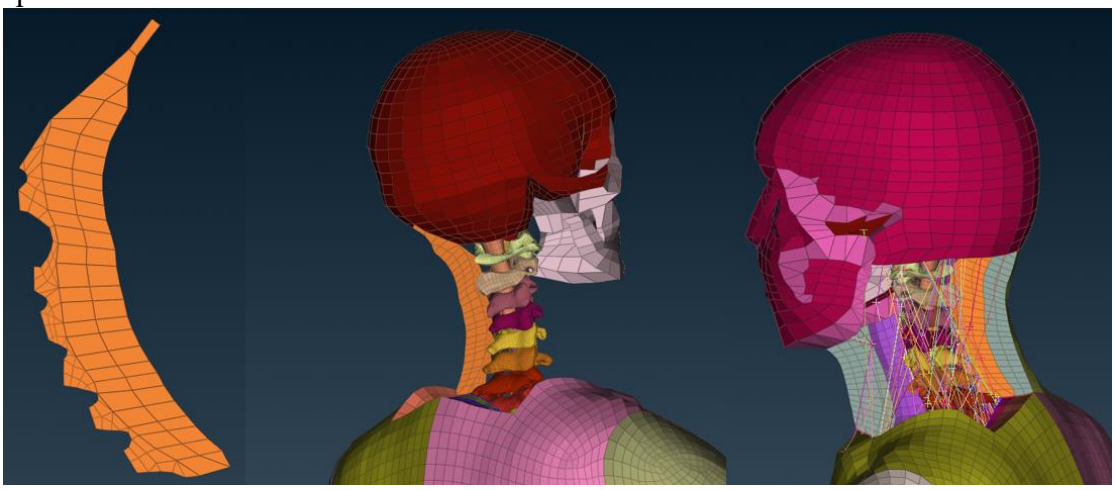

Figure 32: The nuchal ligament modeling and meshing.

Type: MAT_034: FABRIC
Suffix: <none>
Title: Ligamentum_Nuchae

Row\Col	1	2	3	4	5	6	7	8
1	<Label>	RO F	EA F	EB F		PRBA F	PRAB F	
	800128	1.0E-6	1.0E-6	1.0E-6		0.3	0.49	
2	GAB F			CSE F	EL F	PRL F	LRATIO F	DAMP F
	0.0103			1.0	0.001	0.49	0.05	0.05
3	AOPT I	FLC I	FAC I	ELA I	LNRC F	FORM F	FVOPT F	TSRFAC I
	0.0	0.0	0.0	0.0	0.0	14.0	0.0	0
4		RGBRTH F	A0REF I	A1 F	A2 F	A3 F	X0 F	X1 F
		0.0	0	0.0	0.0	0.0	0.0	0.0
5	V1 F	V2 F	V3 F	D1 F	D2 F	D3 F	BETA F	
	0.0	0.0	0.0	0.0	0.0	0.0	0.0	
6	LCA I	LCB I	LCAB I	LCUA I	LCUB I	LCUAB I	RL F	
	760939	760940	0	0	0	0	0.0	

Figure 33: The material card of the nuchal ligament.

Then, the updated geometry was run in both ROM and Kang simulations using the updated parameters (Combination No: 7) in Objective-2 and -3.

7.2 Updated Model Geometry in ROM Simulations

Geometrically updated SHBM was used in ROM simulations. The neck moment vs angle results obtained from the two simulations using the updated model are presented in comparison with both the SHBM nominal data and ROM experimental results in Figure 34.

The results indicate that the updated neck lobe had no impact on neck moment vs angle values. In contrast, the inclusion of the nuchal ligament led to an increase in neck moment values during both extension and flexion. Notably, the ligament's resistance to flexion introduced a fluctuation in the moment response.

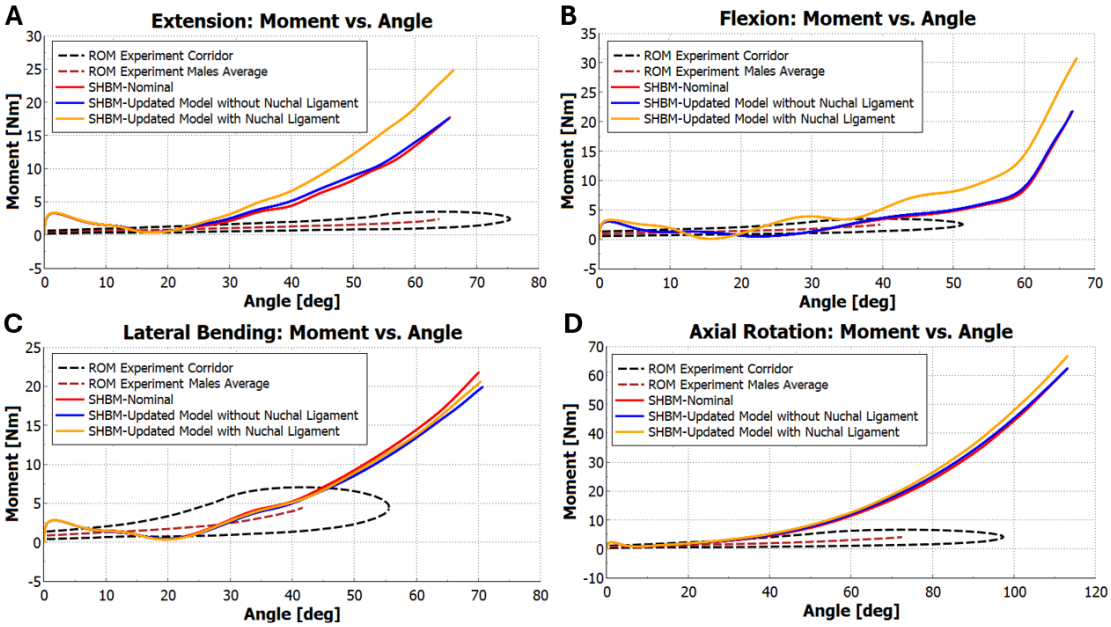

Figure 34: Neck moment values comparison of updated model, SHBM nominal and ROM experiments. A: Extension. B: Flexion. C: Left lateral bending. D: Left axial rotation.

As previously mentioned, the nuchal ligament connects the cervical vertebrae to the skull, potentially influencing the segmental angular contributions during ROM. To investigate this effect, the angular contributions of the cervical segments in the updated model are compared with both the SHBM nominal data and the results reported by (Lindenmann et al. 2022), as shown in Figure 35. Accordingly, while mesh refinement in the neck lobe had no significant impact on the segmental angular contributions, the inclusion of the nuchal ligament resulted in noticeable changes during extension and flexion, as expected.

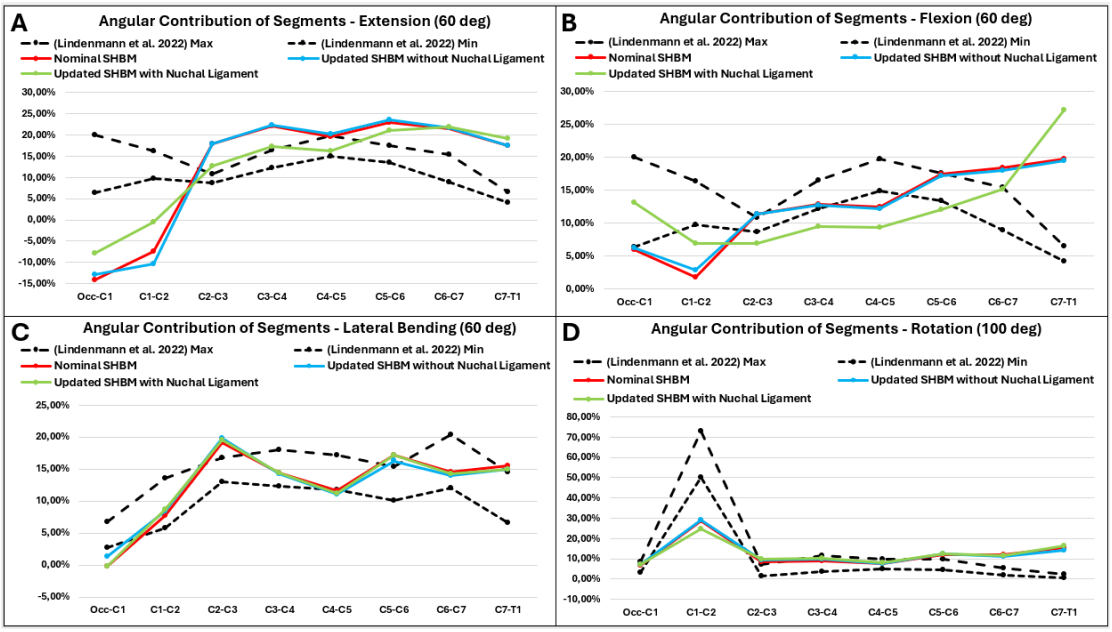

Figure 35: Segments angular contribution comparison of updated model, nominal SHBM and (Lindenmann et al. 2022) results. A: Extension. B: Flexion. C: Lateral bending. D: Axial rotation.

Neck Combination No: 7, identified as one of the most promising material configurations, was also tested with the updated geometry. The updated model, which initially exhibited a stiffer neck response compared to the nominal SHBM, was substantially softened with the application of Neck Combination No: 7 materials, yielding results closely aligned with those of the average male (see Figure 36). Notably, these outcomes were nearly identical to those obtained when applying Neck Combination No: 7 to the original geometry, except in the flexion scenario. In flexion, the presence of the nuchal ligament increased resistance, thereby slightly stiffening the neck response. This provided a beneficial effect, as the flexion response, initially too soft when Neck Combination No: 7 was applied to the original geometry, became more aligned with averaged male results (see Appendix Figure A 7 for 2000ms ROM simulations).

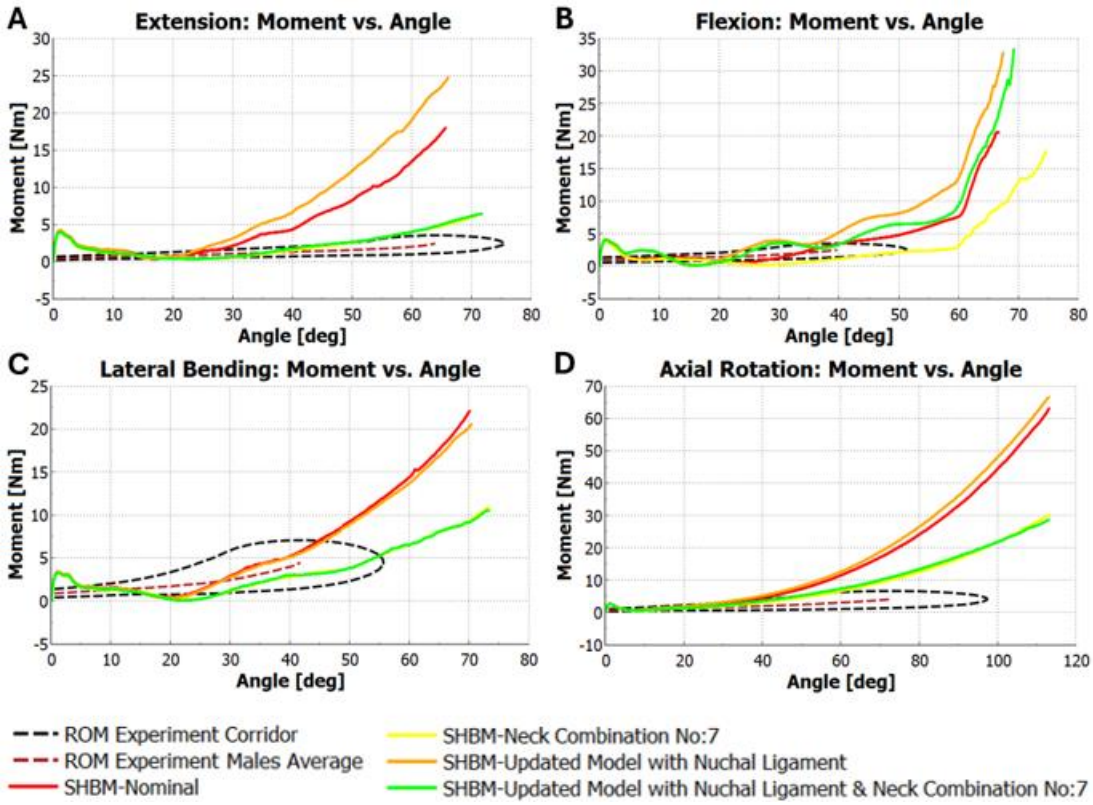

Figure 36: Effect of Neck Combination No: 7 to updated geometry in ROM. A: Extension. B: Flexion. C: Left lateral bending. D: Left axial rotation.

7.3 Updated Model Geometry in Kang Simulations

Geometrically updated SHBM model was implemented in Kang simulations in this section. Truncated SHBM for both oblique and twist impacts was prepared. Subsequently, three simulations were conducted to investigate the effects of the nuchal ligament and the findings from the parameter study: (1) a model excluding the nuchal ligament, aimed at evaluating the impact of mesh refinement in the neck lobe; (2) a model including the nuchal ligament, to assess its specific contribution to overall biomechanical behavior; and (3) a model including the nuchal ligament combined with the most promising material set (Combination No: 7), to evaluate the results of the parameter study.

The results for the oblique impact scenario are presented in Figure 37. The updated neck lobe demonstrated behavior closely aligned with that of the nominal model. The inclusion of the nuchal ligament resulted in a slightly stiffer neck response compared to the nominal model up to the onset of rebound. Finally, when Neck Combination No: 7 was applied to the neck flesh and neck skin components, the model exhibited a slightly stiffer response than the nominal SHBM prior to rebound.

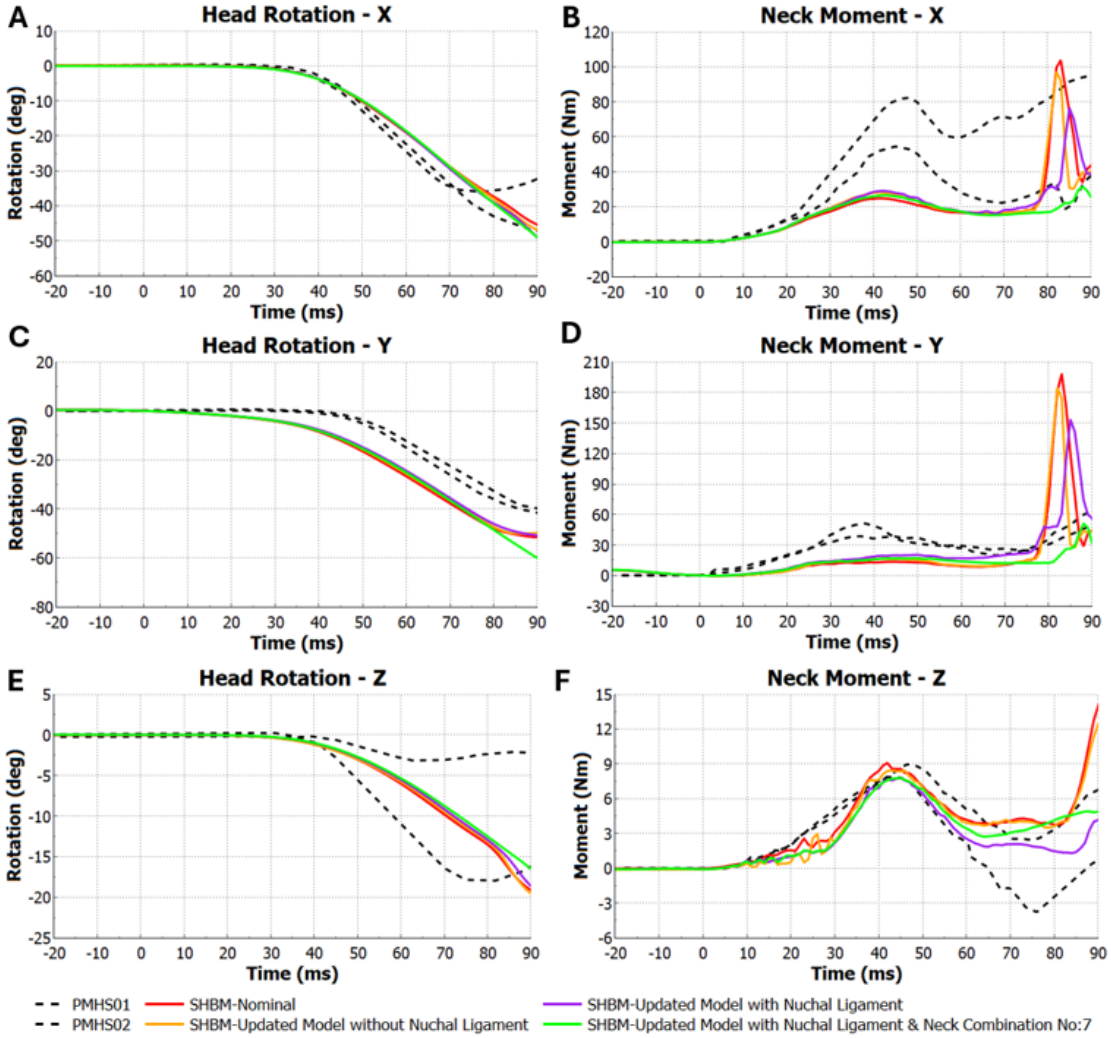

Figure 37: Evaluation of updated geometry and most promising material models in the oblique scenario. Head rotation; A: x-axis, C: y-axis, E: z-axis. Lower neck moment; B: x-axis, D: y-axis, F: z-axis.

For the twist scenario, the updated geometry produced a neck response closely matching that of the nominal SHBM without the nuchal ligament (see Figure 38). The inclusion of the nuchal ligament increased neck moment values. In contrast, when Neck Combination No: 7 materials were applied to the model with the nuchal ligament, the neck response became less stiff and more consistent with the PMHS response.

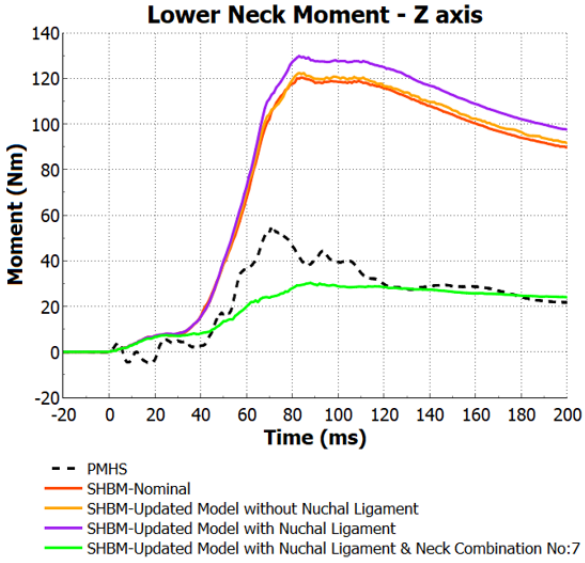

Figure 38: Evaluation of updated geometry and most promising material models in the twist scenario.

7.4 Updated Model Geometry Discussion

Upon examining the model with updated geometry, it is observed that it yields results closer to the nominal SHBM in both the ROM and Kang simulations. The inclusion of the nuchal ligament slightly increases the stiffness of the neck response, which had been overly softened by the updated parameter set (Combination No: 7) in ROM flexion, resulting in moment outputs more closely aligned with the ROM experiment males average. However, in terms of intervertebral rotation, the model with updated geometry demonstrates less improvement compared to the configuration employing the original geometry with the updated parameters. This reduced performance is primarily attributed to the termination of the nuchal ligament at C7, which led to an excessive increase in angular rotation between C7 and T1. Consequently, the model with updated geometry will not be considered for further validation simulations.

8 Objective-5: Validation in Low-to-High Speed Crash Scenarios

In this section, two simulations, representing low-speed and high-speed crash scenarios, are conducted to validate the findings presented in Objectives-2 and -3, as well as to assess the performance of the updated biofidelic parameters. Accordingly, original geometry with Combination No: 7 was selected as the most promising parameters and named as "Updated Parameters" in this section.

For the low-speed validation, the study titled "Kinematic Comparison Between the THOR Dummy, Older Volunteers, and Older PMHS in Low-Speed Non-Injurious Frontal Impacts" by (Lopez-Valdez et al. 2017) was replicated using the SHBM.

For the high-speed validation, the SHBM was used to simulate the study "Impact Response of Restrained PMHS in Frontal Sled Tests: Skeletal Deformation Patterns Under Seat Belt Loading" by (Shaw et al. 2009).

8.1 Methodology

In both experiments, sled tests conducted with PMHS were simulated using SHBM. Subsequently, the head and T1 displacements, as well as the forces measured on the upper and lower shoulder belts, were compared among the nominal SHBM, the SHBM with updated parameters, and the experimental PMHS data.

8.1.1 Low-speed -9km/h- sled test setup and boundary conditions

A previously developed boundary condition model, (Larsson 2020) Figure 39, was used. The full-body SHBM was positioned to the same positioning target used in (Larsson 2020) then belted. A prescribed acceleration pulse was applied to the sled to replicate the dynamics of a 9 km/h impact.

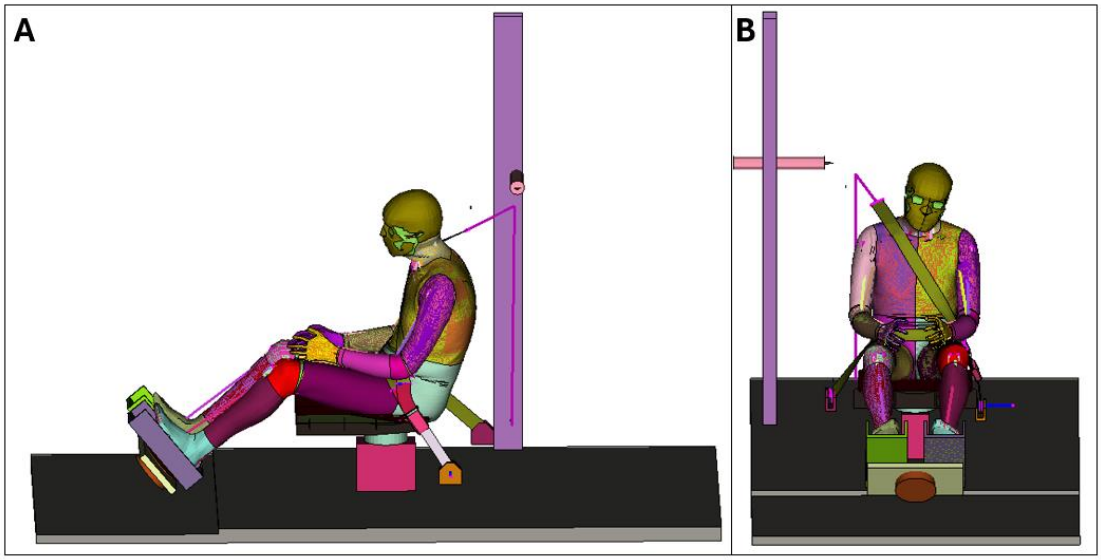

Figure 39: 9km/h sled test setup with SHBM. A: Side view; B: Front view.

The simulation termination time was set to 600 ms. The initial 300 ms were allocated for gravity settling the SHBM with Head CoG and T1 constrained from anterior and lateral displacements. These constraints were released at onset of impact. The actual impact simulation was conducted over the subsequent 300 ms. Accordingly, the 300 ms mark was designated as time zero (0 ms) for all result evaluations.

Two simulations were performed for both the nominal SHBM and the SHBM with updated parameters.

8.1.2 High-speed -40km/h- sled test setup and boundary conditions

A boundary condition model from Chalmers Validation Repository, including pre-defined positioning and seat belt routing, was used, as illustrated in Figure 40. The full-body SHBM was positioned on the seat and the seat belt tightened during the first 350 ms. An acceleration pulse was applied to the sled to simulate a frontal impact at 40 km/h.

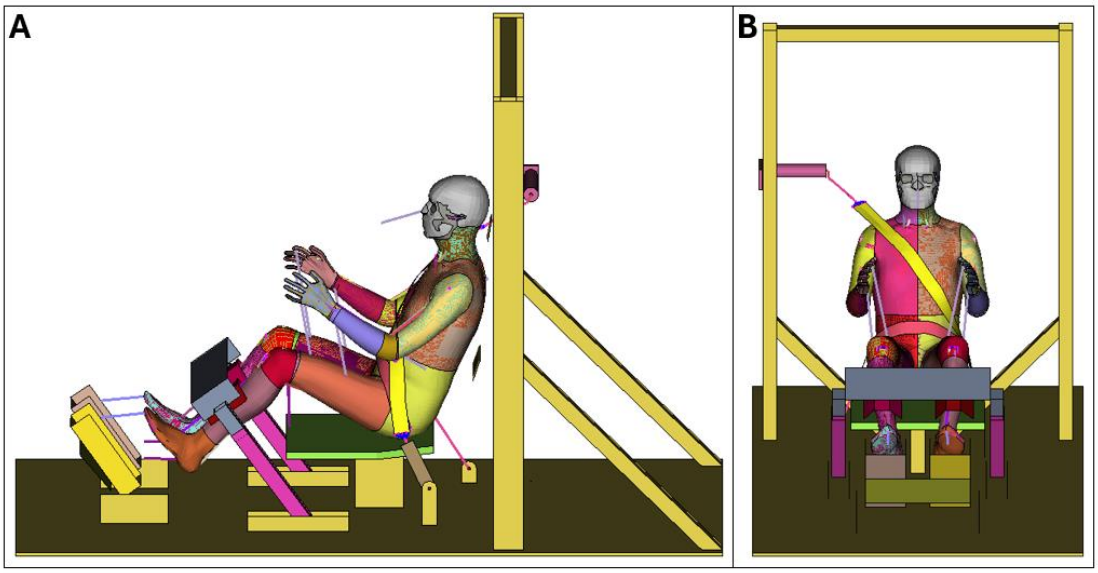

Figure 40: 40km/h sled test setup with SHBM. A: Side view; B: Front view.

The actual impact simulation was carried out during the subsequent 200 ms, with released positioning constraints. As such, the 200 ms mark was designated as time zero (0 ms) for the analysis of the results.

Two simulations were conducted for both the nominal SHBM and the SHBM incorporating the updated parameters.

8.2 Results

As a result of the simulations, head and T1 displacements relative to the moving sleds were extracted along all three axes (X - forwards, Y- lateral right, and Z - down) for both the low-speed and high-speed crash scenarios. Additionally, forces exerted on the upper and lower shoulder belts were calculated to assess loading patterns during impact.

8.2.1 9km/h Impact simulation results

An analysis of the head displacement results, as shown in Figure 41, indicates that the outputs of the nominal SHBM and the SHBM with updated parameters are generally similar. The primary difference is observed in the Z-axis displacement, where the updated model exhibits slightly greater movement. When compared to the PMHS results, both SHBM variants displaced excessively along the Y-axis.

In the case of T1 displacements, the SHBM results align more closely with those of the PMHS. However, a comparison between the nominal SHBM and the updated model reveals that the updated model produces greater displacement along the Y-axis.

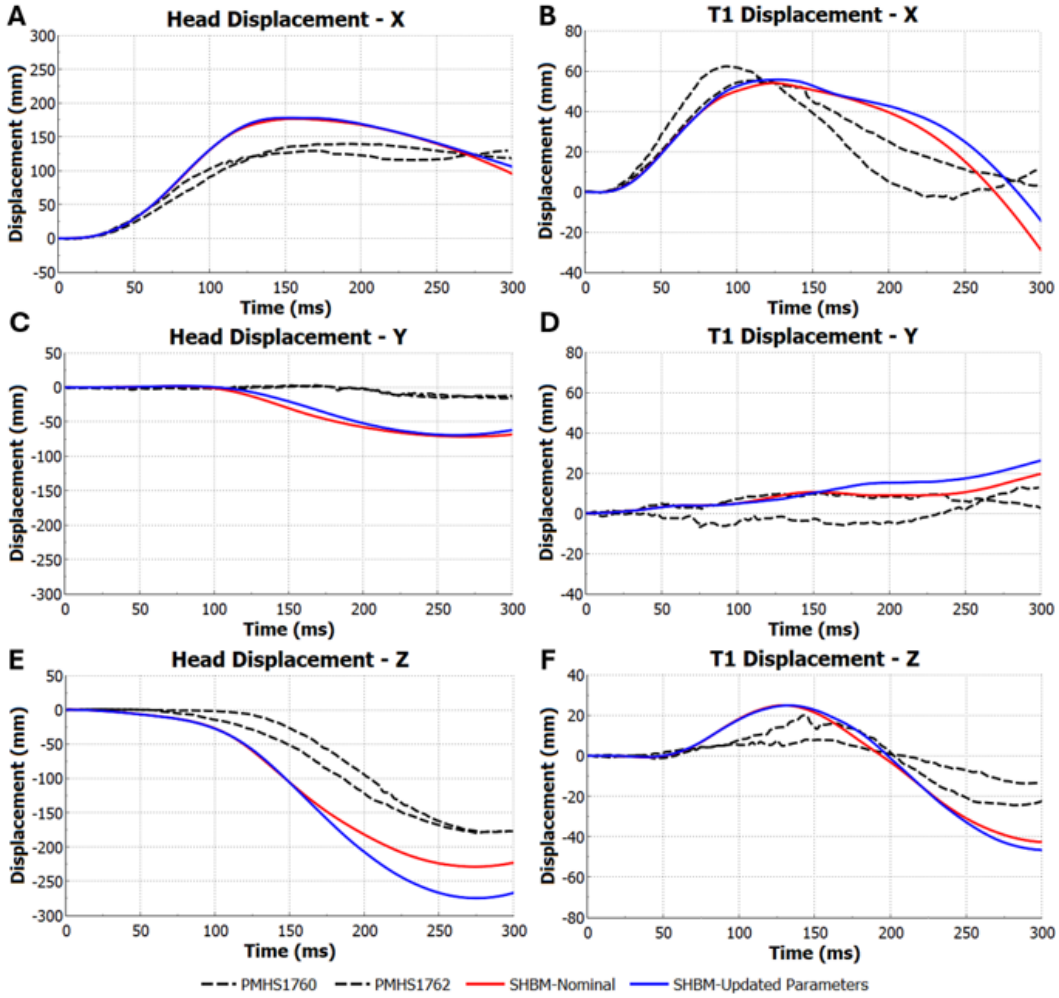

Figure 41: 9km/h sled test head displacements, A: x-axis; C: y-axis; E: z-axis, and T1 displacement, B: x-axis; D: y-axis; F: z-axis.

The comparison of upper and lower shoulder belt forces is presented in Figure 42. The results indicate that both the nominal SHBM and the SHBM with updated parameters produced force outputs that closely matched those of PMHS1762 for both the upper and lower shoulder belts.

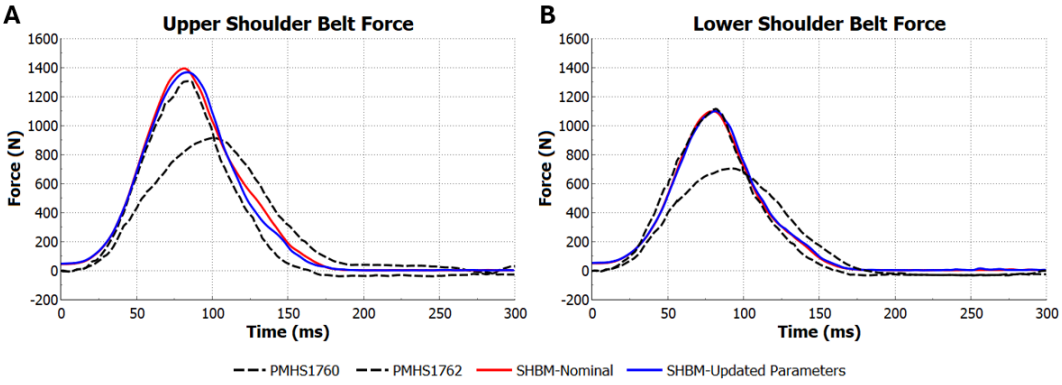

Figure 42: 9km/h sled test shoulder belt forces, A: Upper; B: Lower

8.2.2 40km/h Impact simulation results

When the displacement results presented in Figure 43 are examined, it is observed that both the nominal SHBM and the updated parameterized SHBM yield results that fall within or close to the corridor defined by the standard deviation of the PMHS mean. However, displacements of the head and T1 along the Z-axis exhibited greater deviations toward the end of the simulation compared to the PMHS test corridor.

Additionally, only slight differences were observed between the nominal and updated SHBM in the head displacements along both the Y- and Z-axes.

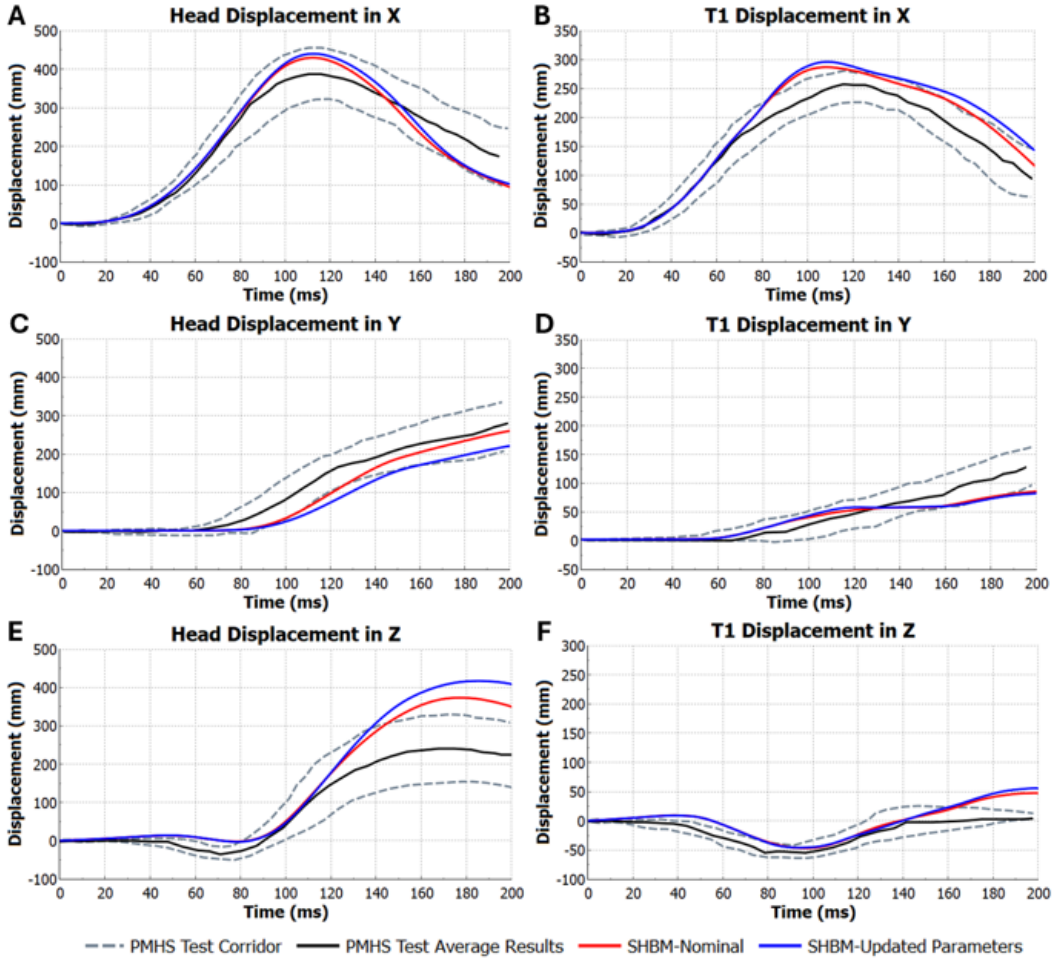

Figure 43: 40km/h sled test head displacements, A: x-axis; C: y-axis; E: z-axis, and T1 displacement, B: x-axis; D: y-axis; F: z-axis.

When the upper and lower shoulder forces are compared, it is observed that the nominal SHBM and the parameter-updated SHBM yield very similar results. As illustrated in Figure 44, although both SHBMs produce higher peak shoulder forces compared to the PMHS data, their force responses align closely with the experimental values throughout the remainder of the test.

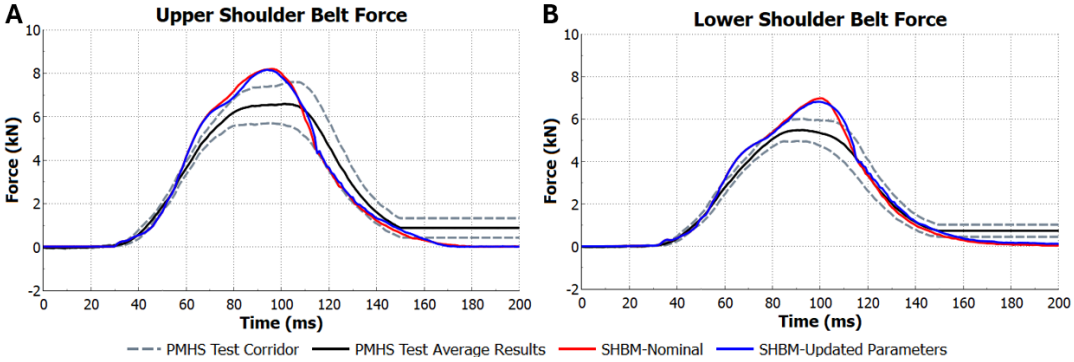

Figure 44: 40km/h sled test shoulder belt forces, A: Upper; B: Lower.

9 Discussion

In this thesis, 5 objectives were achieved to validate the biofidelity of the neck soft tissue of SHBM.

9.1 Modeling ROM Experiments with SHBM for Tuning Neck Soft Tissue Modeling

In the ROM experiments, participants' back contours were measured using flexible rulers, and head–neck positioning was adjusted accordingly. As a result, individual variations in back shape led to subject-specific head–neck orientations. This introduced a limitation in the standardization of the SHBM's head–neck positioning. In the simulations, a seated SHBM was used for alignment. Establishing a representative head–neck posture based on anthropometric data of the average male and applying it uniformly to the SHBM may enable more consistent and reliable comparisons between experimental and simulation outcomes.

Conducting the ROM simulations with a relatively short duration of 600 ms, compared to ROM experiments duration (6-10 s), introduced noticeable inertial effects at the onset of motion. However, this influence was confined to the initial phase and did not significantly affect the overall results. These findings suggest that, for quasi-static movements such as ROM, running simulations at higher speeds while disregarding initial inertial discrepancies may be an acceptable trade-off for achieving reduced computation times.

The simulation results indicated that the SHBM exhibited a stiffer neck response in especially extension and axial rotation compared to the ROM experiment males average results. This discrepancy can be attributed to the stiffness of neck soft tissue within the SHBM. Additionally, modeling the neck musculature with both beam elements and solid flesh components likely resulted in a redundancy in stiffness representation (see Section 4.2 and Figure 9). When the neck lobe representing skin, passive muscle and fat tissues was removed from the model, it was seen that the muscle beam elements represented the passive muscle properties well. To improve the physiological accuracy of the model's neck behavior, it is essential to eliminate this overlap and avoid duplicative characterization of muscle structures. Removing the neck lobe from the SHBM can yield a neck moment values similar to that of the ROM experiment males average. Nevertheless, one of the main uses of the SHBM is for virtual occupant safety simulations (Pipkorn et al. 2023), in which it is essential to establish contact surfaces between the body and occupant protection systems such as seat belts and airbags. Moreover, the biofidelity of the SHBM should be preserved. Therefore, removing the neck lobe cannot be a solution.

9.2 Parameter Study to Investigate the Contributions of the Neck Soft Tissue Modeling on Neck ROM

The parameter studies demonstrated that modeling the neck skin in a slack state effectively reduced the stiffness-enhancing influence of the skin. This approach accounts for the possibility that, in a neutral (or "free") posture, the neck skin may already be partially compressed. Furthermore, the viscoelastic nature of skin, exhibiting strain-rate dependent stress–strain behavior, was incorporated by implementing a

material model that assigns different stress–strain curves according to the applied strain rate. These enhancements collectively contributed to a notable reduction in neck moment values in the low-acceleration ROM simulations and high acceleration Kang twist simulations, but little influence in the high-acceleration Kang oblique simulations.

The (Naseri 2022) alternative adipose (Trial No: 6) neck flesh model yielded moments that exceeded the ROM experiment males average values, suggesting that the material was too stiff for anatomical accuracy. Utilizing the (Naseri 2022) soft adipose version led to improved results in terms of reduced neck moments. Additionally, setting the Poisson's ratio to 0.49 further aided in softening the response. In contrast, using more compressible values (e.g., 0.45) produced neither meaningful softening nor accurately reflected physiological tissue behavior. Also reducing the shear modulus (Combination No: 2) has a limited effect on the overall stiffness response in the (Naseri 2022) soft adipose model.

When (Panzer et al. 2024) material properties such as skin, adipose tissue, and muscle were applied to SHBM, the neck response became excessively stiff.

The application of compressible materials, such as cushion foams, around the cervical region also contributed to a reduction in neck moment values. The goal was to model the passive soft tissue that surrounds the cervical vertebrae, thereby preserving anatomical shape and volume, without redundantly representing muscle behavior already included through beam elements. This strategy effectively reduced artificial stiffness while maintaining structural integrity. However, the instability of the cushion foam neck flesh model in high-acceleration Kang simulations caused this material model not to be selected as the final choice.

Segmental angular contribution analysis further revealed that the soft tissue surrounding the neck, particularly the neck flesh, limited proper angular motion at the Occ–C1 and C1–C2 junctions, during extension and flexion. This finding indicates that the current neck flesh material may still be stiffer than physiologically appropriate, constraining the natural articulation of the upper cervical spine.

When the updated parameters (Combination No: 3 or 7) were applied in the ROM simulations, analysis of segmental angular contributions revealed significant improvements in extension and flexion. This improvement can be explained by the reduced compression exerted by the softened neck flesh on the cervical vertebrae, particularly in the upper cervical spine, as compared to the nominal model configuration.

9.3 Evaluation and Calibration for High Acceleration Scenarios

Nominal SHBM compared to SHBM without neck lobe indicates that the presence of the neck lobe in the SHBM alters the overall neck response under high-acceleration conditions. In the twist scenario, inclusion of the neck lobe produced neck moment values significantly higher than those observed in the PMHS tests, while its exclusion resulted in considerably lower values.

Similar results were observed in the oblique scenario. However, unlike here, sudden changes in moment values were observed after the 80th ms. These deviations were

attributed to the head rigid boundary condition, which resulted in a rebound effect. The PMHS in the experiment did not impact the ring. Consequently, data beyond 80 ms were considered unreliable for direct comparison with PMHS results. To capture both the pre-impact state and the onset of rebound behavior, the time window from -20 ms to 90 ms was selected for the subsequent analyses.

Comparison with the PMHSs test results revealed that all trials exhibited lower stiffness than expected in the x-axis (lateral bending) and y-axis (extension/flexion). In contrast, the response in the z-axis (axial rotation) was more consistent with the experimental data. However, given that the oblique scenario involves a combination of all neck motions, the twist scenario provides a more isolated and thus more reliable assessment of axial rotational behavior.

The results of the parameter study based on Kang simulations indicated that the updated soft tissue parameters did not lead to substantial improvements under high acceleration loading conditions. However, they did not adversely affect neck reactions during high-acceleration simulations, suggesting that parameter tuning aimed at low-speed performance does not necessarily compromise performance in higher-speed scenarios. Similarly, parameter calibration specifically targeting high-acceleration conditions failed to yield meaningful enhancements. In particular, increasing the stiffness of the stress–strain curves at the highest strain-rate level within the rate-dependent neck skin model did not result in a stiffer neck response. On the other hand, modifying the lowest strain-rate behavior can help to cover even slower motions. Therefore, the calibrated parameters (Combination No: 7) were the most promising parameters.

9.4 Updating the Model Geometry

Based on the studies conducted up to this point, it was observed that the SHBM exhibited overly stiff neck responses during low-acceleration motions and excessively soft responses during high-acceleration motions. Following the parameter study, updates were implemented to soften the neck response for low-acceleration conditions. Although this led to reduced stiffness as intended, the resulting flexion response became even softer than the average values observed in ROM experiments with male subjects. At the same time, the modifications did not yield significant improvements for high-acceleration scenarios.

To address these limitations, an updated neck geometry was developed. The redesigned neck lobe aimed to enhance both anatomical accuracy and dynamic response characteristics. Specifically, increasing the neck flesh thickness and incorporating the nuchal ligament contributed to increased neck moment values. To counterbalance this effect and maintain low-speed performance, the parameter study's optimized material properties (Combination No: 7) were applied to the updated geometry. As a result, the model produced sufficiently soft responses under low-acceleration loading, while the inclusion of the nuchal ligament hardens the flexion. Additionally, a slight improvement (increase) in the lower neck moment values was achieved for high-acceleration conditions.

When analyzing the angular contribution of cervical segments, it was found that the nuchal ligament notably influenced motion in both extension and flexion. However, this influence did not consistently translate into improvements. In particular, the ligament’s termination at C7 increased the relative motion between C7 and T1, leading

to less favorable outcomes in the lower cervical spine. While improvements were observed in the upper cervical segments (Occ–C2), the kinematic performance of the lower segments (C7–T1) deteriorated, highlighting the need for further refinement in ligament modeling and geometric transitions. For this reason, it was decided not to use the model with updated geometry in the validation phase. However, it should be taken into consideration that the nuchal ligament could increase biofidelity by providing better head-neck responses with better meshing and correct attachment in future studies.

9.5 Validation in Low-to-High Speed Crash Scenarios

To validate the updated SHBM configurations developed during the parameter study, two separate sled test simulations were conducted under low- and high-speed conditions. In the low-speed impact scenario, the updated SHBM produced results that were largely consistent with those of the nominal model. The most notable discrepancies were observed in T1 displacement in the Y-direction and head displacement in the Z-direction. These differences are attributed to the softer neck structure in the updated model, which allowed for slightly increased flexion under the weight of the head.

In the high-speed sled test, the simulation outcomes of the nominal and updated models showed even closer agreement. The primary variations were again observed in head displacements in both the y- and z-directions. As in the low-speed case, the increased flexion resulting from the softer neck contributed to these differences. Overall, these findings suggest that the neck softening applied in the updated model does not significantly alter global kinematic responses under impact loading and remains within acceptable bounds for both low- and high-speed conditions.

9.6 Limitations and Future Work

In the ROM simulations, the exact head–neck positioning of the subjects was not available, leading to the use of estimated alignment for the SHBM. For improved accuracy, acquiring representative head–neck positioning data from an average male population could enhance the validity of the simulation setup.

In the Kang oblique simulations, the head's impact with the rigid boundary condition caused a pronounced rebound. While such contact is expected under oblique loading (it was similar with SHBM v11.0.0), its occurrence as early as 80 ms substantially limits the meaningful interpretation of the remaining portion of the 200 ms simulation. Therefore, revising the Kang oblique simulation setup could enhance the utility of the test.

Despite the improvements achieved in low-acceleration responses, the updated SHBM did not exhibit significant enhancements under high-acceleration conditions. Given that many experimental validation tests involve high-acceleration impacts, further work in this area is warranted. In particular, the development of a more refined strain-rate dependent neck skin model may contribute to more realistic dynamic behavior.

Future studies could also explore the use of alternative soft materials, such as cushion foam, for modeling neck flesh to further reduce neck moment values without compromising anatomical fidelity.

Finally, improved meshing of the nuchal ligament may lead to more accurate segmental angular motion and stiffer neck responses in flexion.

10 Conclusion

The current version of the SHBM (v11.1.0) exhibits overly stiff neck responses during low-acceleration movements across the full range of motion. Conversely, it demonstrates excessively soft neck responses under high-acceleration conditions, such as those observed in Kang simulations.

The implementation of a strain-rate dependent neck skin model, incorporating both variable stiffness and slack characteristics, contributed to a reduction in neck moment values in low-acceleration ROM scenario. Similarly, applying the (Naseri 2022) soft adipose tissue model with a lowered Poisson's ratio (0.49) also led to a decrease in stiffness. The combination of these two approaches further enhanced the softening of the neck response under low-acceleration loading and in the high-acceleration neck twist scenario, resulting in results closer to the experimental results with updated neck lobe material parameters. Negligible effect of neck lobe material parameters was observed in the high-acceleration (Kang) oblique scenario, and only small differences in head excursion results between updated and nominal SHBM were observed in the two full-body validation cases.

The nuchal ligament increased resistance to flexion, and it is recommended to incorporate a nuchal ligament in the SHBM neck in future work.

11 References

Anderst, William, Emma Baillargeon, William Donaldson, Joon Lee, and James Kang. 2013. "Motion Path of the Instant Center of Rotation in the Cervical Spine During In Vivo Dynamic Flexion-Extension: Implications for Artificial Disc Design and Evaluation of Motion Quality After Arthrodesis." *Spine* 38 (10): E594–601. https://doi.org/10.1097/BRS.0b013e31828ca5c7.

Barker, Jeffrey B., Duane S. Cronin, and Naveen Chandrashekar. 2014. "High Rotation Rate Behavior of Cervical Spine Segments in Flexion and Extension." *Journal of Biomechanical Engineering* 136 (12): 121004. https://doi.org/10.1115/1.4028107.

Brolin, Karin, Peter Halldin, and Ingrid Leijonhufvud. 2005. "The Effect of Muscle Activation on Neck Response." *Traffic Injury Prevention* 6 (1): 67–76. https://doi.org/10.1080/15389580590903203.

Chazal, J., A. Tanguy, G. Gaurel, G. Escande, M. Guillot, and G. Vanneuville. 1985. "Biomechanical Properties of Spinal Ligaments and a Histological Study of the Supraspinal Ligament in Traction."

Cronin, Duane S., Dilaver Singh, Donata Gierczycka, Jeffery Barker, and David Shen. 2018. "Modeling the Neck for Impact Scenarios." In *Basic Finite Element Method as Applied to Injury Biomechanics*, 503–38. Elsevier. https://doi.org/10.1016/B978-0-12-809831-8.00013-1.

Deng, Yih-Charng, Xiaowei Li, and Yi Liu. 1999. "Modeling of the Human Cervical Spine Using Finite Element Techniques." In , 1999-01–1310. https://doi.org/10.4271/1999-01-1310.

Drake, Richard L., A. Wayne Vogl, and Adam W.M. Mitchell. 2014. "Head and Neck." In *Gray's Anatomy*. Third Edition. Churchill Livingstone.

Fice, Jason B., Duane S. Cronin, and Matthew B. Panzer. 2011. "Cervical Spine Model to Predict Capsular Ligament Response in Rear Impact." *Annals of Biomedical Engineering* 39 (8): 2152–62. https://doi.org/10.1007/s10439-011-0315-4.

Forman, Jason, Gerald S. Poplin, C. Greg Shaw, Timothy L. McMurry, Kristin Schmidt, Joseph Ash, and Cecilia Sunnevang. 2019. "Automobile Injury Trends in the Contemporary Fleet: Belted Occupants in Frontal Collisions." *Traffic Injury Prevention* 20 (6): 607–12. https://doi.org/10.1080/15389588.2019.1630825.

Freeman, Michael D., and Wendy M. Leith. 2020. "Estimating the Number of Traffic Crash-Related Cervical Spine Injuries in the United States; An Analysis and Comparison of National Crash and Hospital Data." *Accident Analysis & Prevention* 142 (July):105571. https://doi.org/10.1016/j.aap.2020.105571.

Gayzik, F. S., D. P. Moreno, C. P. Geer, S. D. Wuertzer, R. S. Martin, and J. D. Stitzel. 2011. "Development of a Full Body CAD Dataset for Computational Modeling: A Multi-Modality Approach." *Annals of Biomedical Engineering* 39 (10): 2568–83. https://doi.org/10.1007/s10439-011-0359-5.

"GHBMC Licensed Model." n.d. *Global Human Body Model Consortium-Owned GHBMC Model, and Elemance as the Exclusive Distributor of the Licensed Model.* (blog). https://www.elemance.com/.

Iraeus, Johan, Karin Brolin, and Bengt Pipkorn. 2020. "Generic Finite Element Models of Human Ribs, Developed and Validated for Stiffness and Strain Prediction – To Be Used in Rib Fracture Risk Evaluation for the Human Population in Vehicle Crashes." *Journal of the Mechanical Behavior of Biomedical Materials* 106 (June):103742. https://doi.org/10.1016/j.jmbbm.2020.103742.

Jolivet, Erwan, Yoann Lafon, Philippe Petit, and Philippe Beillas. 2015. “Comparison of Kriging and Moving Least Square Methods to Change the Geometry of Human Body Models.” In , 2015-22–0013. https://doi.org/10.4271/2015-22-0013.

Kang, Y-S, J Stammen, K Moorhouse, and J Bolte Iv. 2018. “Head and Neck Responses of Post Mortem Human Subjects in Frontal, Oblique, Side and Twist Scenarios.”

Kohan, Emil J., and Garrett A. Wirth. 2014. “Anatomy of the Neck.” *Clinics in Plastic Surgery* 41 (1): 1–6. https://doi.org/10.1016/j.cps.2013.09.016.

Larsson, E. 2020. “SAFER HBM in 9kph Sled Simulations - Selection of Torso Skin and Flesh Material Properties.”

———. 2021. “Towards a Human Body Model for Prediction of Vehicle Occupant Kinematics in Omni-Directional Pre-Crash Events.”

Lindenmann, Sara, Christos Tsagkaris, Mazda Farshad, and Jonas Widmer. 2022. “Kinematics of the Cervical Spine Under Healthy and Degenerative Conditions: A Systematic Review.” *Annals of Biomedical Engineering* 50 (12): 1705–33. https://doi.org/10.1007/s10439-022-03088-8.

Liu, Mingyue, Ryan D. Quarrington, Baptiste Sandoz, William S. P. Robertson, and Claire F. Jones. 2024a. “Evaluation of Apparatus and Protocols to Measure Human Passive Neck Stiffness and Range of Motion.” *Annals of Biomedical Engineering* 52 (8): 2178–92. https://doi.org/10.1007/s10439-024-03517-w.

Liu, Mingyue, Ryan D. Quarrington, Baptiste Sandoz, William S.P. Robertson, and Claire F. Jones. 2024b. “Neck Stiffness and Range of Motion for Young Males and Females.” *Journal of Biomechanics* 168 (May):112090. https://doi.org/10.1016/j.jbiomech.2024.112090.

Lopez-Valdez, F.J, D. Hynd, and M. Wisch. 2017. “SAFETY ENHANCED INNOVATIONS FOR OLDER ROAD USERS, D2.3, Kinematic Comparison between the THOR Dummy, Older Volunteers and Older PMHS in Low-Speed Non-Injurious Frontal Impacts.”

McCuller, Christopher, Rishita Jessu, and Avery L. Callahan. 2023. “Physiology, Skeletal Muscle.” National Library of Medicine. 2023. https://www.ncbi.nlm.nih.gov/books/NBK537139/.

Naseri, H. 2022. “Calibration of Adipose Tissue Material Properties in LS-DYNA.”

Ní Annaidh, Aisling, Karine Bruyère, Michel Destrade, Michael D. Gilchrist, Corrado Maurini, Melanie Otténio, and Giuseppe Saccomandi. 2012. “Automated Estimation of Collagen Fibre Dispersion in the Dermis and Its Contribution to the Anisotropic Behaviour of Skin.” *Annals of Biomedical Engineering* 40 (8): 1666–78. https://doi.org/10.1007/s10439-012-0542-3.

Östh, Jonas, Karin Brolin, and Dan Bråse. 2015. “A Human Body Model With Active Muscles for Simulation of Pretensioned Restraints in Autonomous Braking Interventions.” *Traffic Injury Prevention* 16 (3): 304–13. https://doi.org/10.1080/15389588.2014.931949.

Ottenio, Mélanie, Doris Tran, Aisling Ní Annaidh, Michael D. Gilchrist, and Karine Bruyère. 2015. “Strain Rate and Anisotropy Effects on the Tensile Failure Characteristics of Human Skin.” *Journal of the Mechanical Behavior of Biomedical Materials* 41 (January):241–50. https://doi.org/10.1016/j.jmbbm.2014.10.006.

Panzer, M, A Caudillo, and B Gepner. 2024. “Developing and Implementing New Flesh Materials Based on Human Tissue Data for GHBMC M50-O.”

Pipkorn, Bengt, Lotta Jakobsson, Johan Iraeus, and Jonas Östh. 2023. “THE SAFER HBM – A HUMAN BODY MODEL FOR SEAMLESS INTEGRATED OCCUPANT ANALYSIS FOR ALL ROAD USERS.”

Pipkorn, Bengt, Jonas Östh, Erik Brynskog, Emma Larsson, Liselotte Rydqvist, Johan Iraeus, Daniel Perez-Rapela, and Lotta Jakobsson. 2021. “Validation of the SAFER Human Body Model Kinematics in Far-Side Impacts.”

“Research Project.” n.d. *Advancing Neck Injury Prediction in Car Crashes Using the SAFER HBM* (blog). https://research.chalmers.se/en/project/11617.

Shaw, Greg, Dan Parent, Sergey Purtsezov, David Lessley, Jeff Crandall, Richard Kent, Herve Guillemot, Stephen A. Ridella, Erik Takhounts, and Peter Martin. 2009. “Impact Response of Restrained PMHS in Frontal Sled Tests: Skeletal Deformation Patterns Under Seat Belt Loading.” In , 2009-22–0001. https://doi.org/10.4271/2009-22-0001.

Shigeta, Kenji, Yuichi Kitagawa, and Tsuyoshi Yasuki. 2009. “DEVELOPMENT OF NEXT GENERATION HUMAN FE MODEL CAPABLE OF ORGAN INJURY PREDICTION.”

Vos, Cees J, Arianne P Verhagen, Jan Passchier, and Bart W Koes. 2008. “Impact of Motor Vehicle Accidents on Neck Pain and Disability in General Practice.” *British Journal of General Practice* 58 (554): 624–29. https://doi.org/10.3399/bjgp08X330762.

World Health Organization. 2023. *Global Status Report on Road Safety 2023*. 1st ed. Geneva: World Health Organization.

Yamashita, Yoshihiro, Hideyuki Uematsu, and Shuichi Tanoue. 2023. “Calculation of Strain Energy Density Function Using Ogden Model and Mooney–Rivlin Model Based on Biaxial Elongation Experiments of Silicone Rubber.” *Polymers* 15 (10): 2266. https://doi.org/10.3390/polym15102266.

Yang, King H., Fuchun Zhu, Feng Luan, Longmao Zhao, and Paul C. Begeman. 1998. “Development of a Finite Element Model of the Human Neck.” In , 983157. https://doi.org/10.4271/983157.

12 Appendix

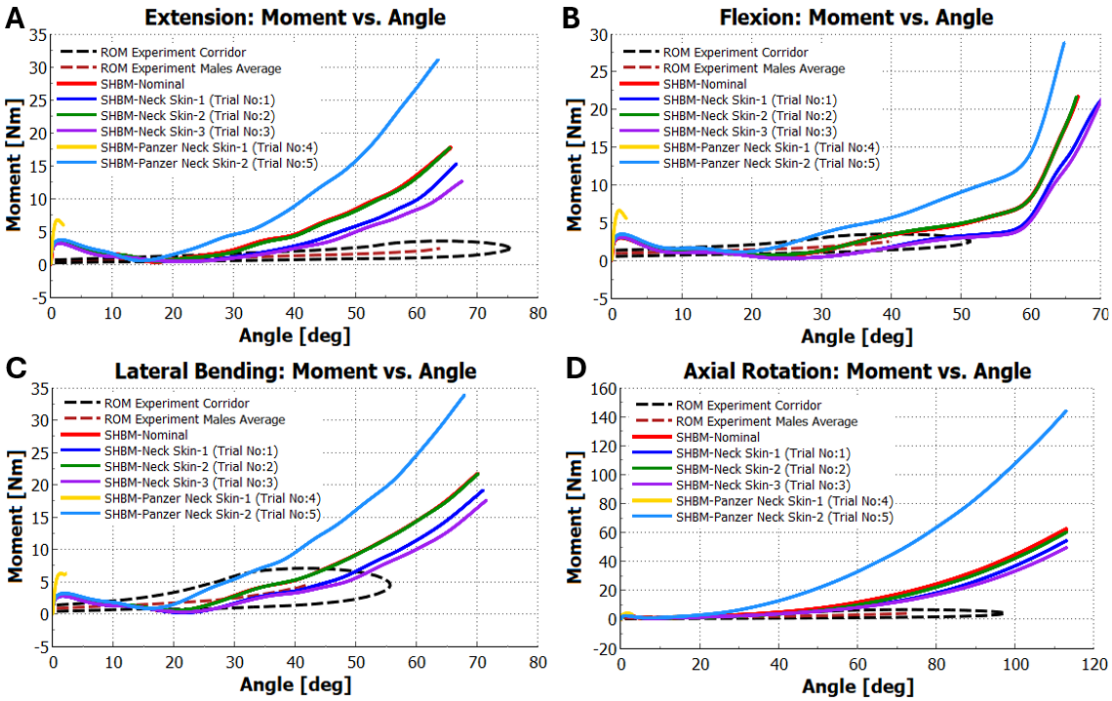

Figure A 1: Neck Skin Parameter Study; A: Extension; B: Flexion; C: Lateral bending; D: Axial rotation.

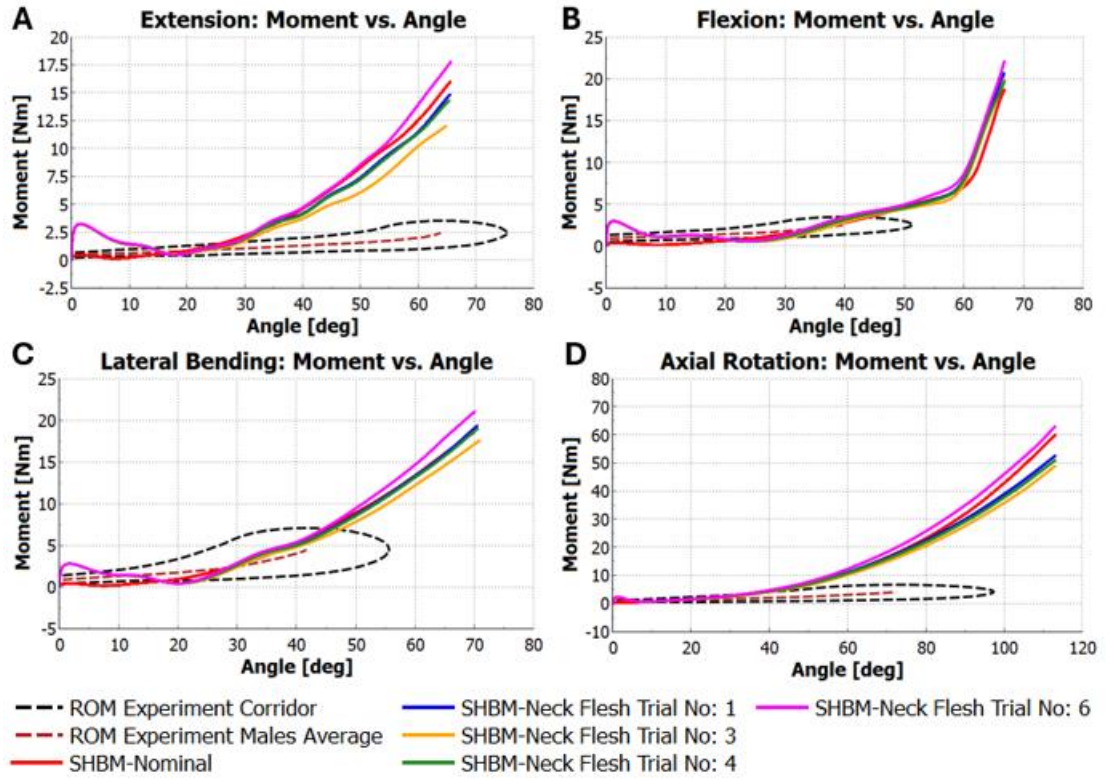

Figure A 2: Neck Flesh Parameter Study with Naseri Adipose Models; A: Extension; B: Flexion; C: Lateral bending; D: Axial rotation.

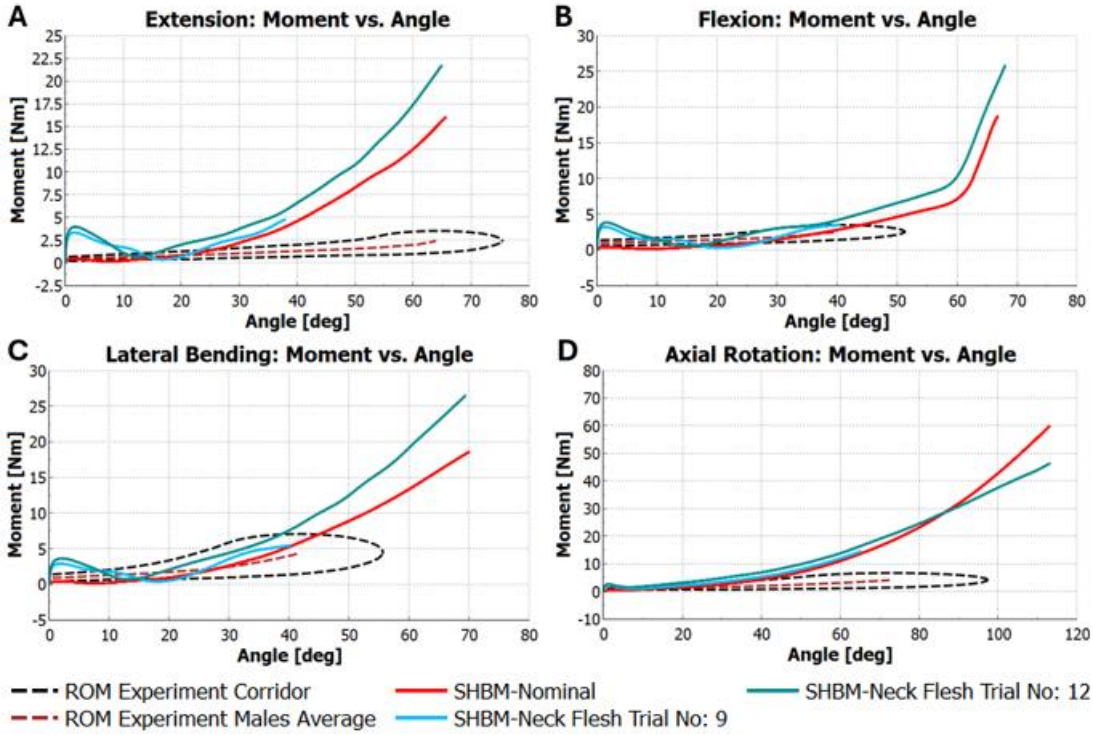

Figure A 3: Neck Flesh Parameter Study with Panzer Adipose and Muscle Models; A: Extension; B: Flexion; C: Lateral bending; D: Axial rotation.

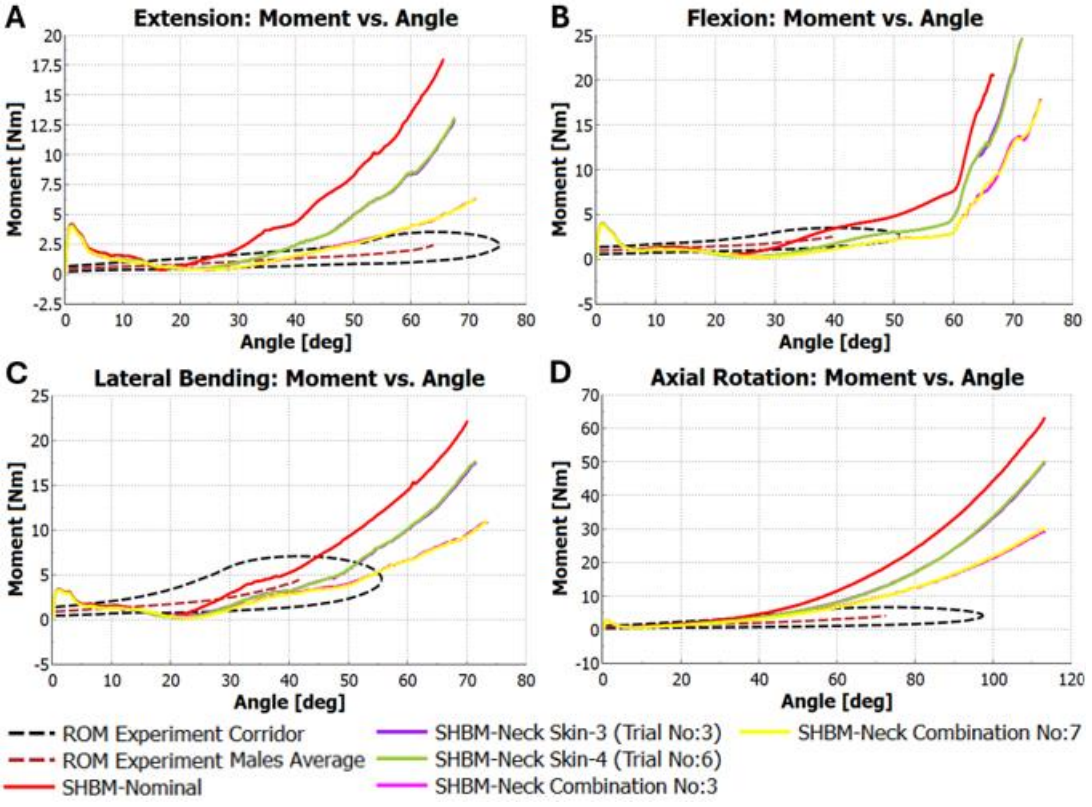

Figure A 4: Comparison of calibrated parameters with the base model; A: Extension; B: Flexion; C: Lateral bending; D: Axial rotation.

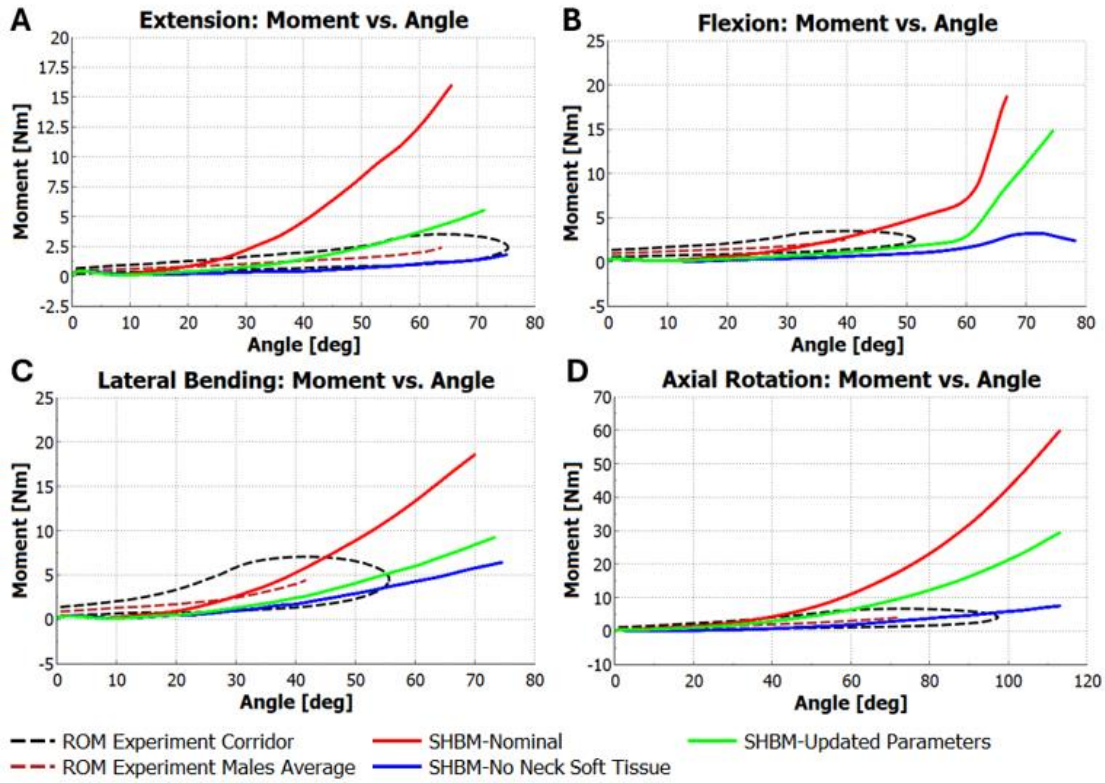

Figure A 5: Effect of using updated parameters (Combination No: 7) in 2000ms ROM simulations; A: Extension; B: Flexion; C: Lateral bending; D: Axial rotation.

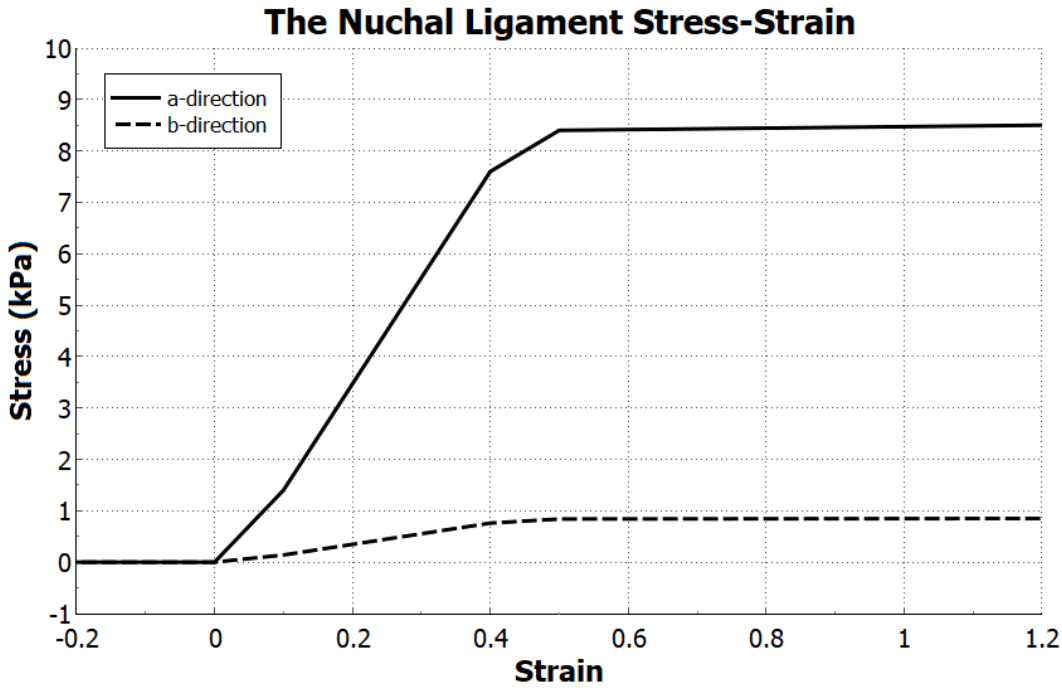

Figure A 6: The nuchal ligament material card stress-strain curves (Chazal et al. 1985)

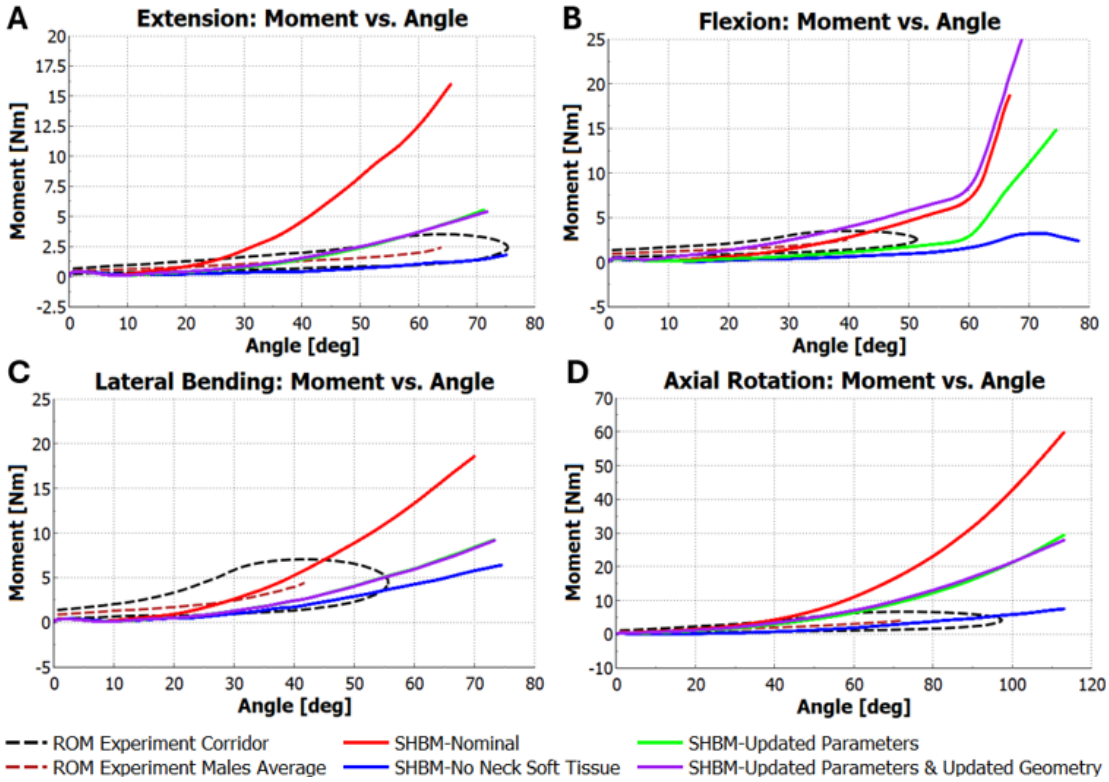

Figure A 7: Effect of using updated geometry with updated parameters (Combination No: 7) in 2000ms ROM simulations; A: Extension; B: Flexion; C: Lateral bending; D: Axial rotation.

DEPARTMENT OF MECHANICS AND
MARITIME SCIENCES,
MOBILITY ENGINEERING
CHALMERS UNIVERSITY OF TECHNOLOGY
Gothenburg, Sweden 2025

CHALMERS
UNIVERSITY OF TECHNOLOGY